# The *in Vivo* Brain Interactome of the Amyloid Precursor Protein*

Yu Bai,[a,b,c] Kelly Markham,[a,b] Fusheng Chen,[a] Rasanjala Weerasekera,[a,d,e] Joel Watts,[a,d] Patrick Horne,[a] Yosuke Wakutani,[a] Rick Bagshaw,[a,d,f] Paul M. Mathews,[g] Paul E. Fraser,[a,h,i] David Westaway,[j] Peter St. George-Hyslop,[a,k,l] and Gerold Schmitt-Ulms[a,d,m]

**Despite intense research efforts, the physiological function and molecular environment of the amyloid precursor protein has remained enigmatic. Here we describe the application of time-controlled transcardiac perfusion cross-linking, a method for the *in vivo* mapping of protein interactions in intact tissue, to study the interactome of the amyloid precursor protein (APP). To gain insights into the specificity of reported protein interactions the study was extended to the mammalian amyloid precursor-like proteins (APLP1 and APLP2). To rule out sampling bias as an explanation for differences in the individual datasets, a small scale quantitative iTRAQ (isobaric tags for relative and absolute quantitation)-based comparison of APP, APLP1, and APLP2 interactomes was carried out. An interactome map was derived that confirmed eight previously reported interactions of APP and revealed the identity of more than 30 additional proteins that reside in spatial proximity to APP in the brain. Subsequent validation studies confirmed a physiological interaction between APP and leucine-rich repeat and Ig domain-containing protein 1, demonstrated a strong influence of Ig domain-containing protein 1 on the proteolytic processing of APP, and consolidated similarities in the biology of APP and p75.** ***Molecular & Cellular Proteomics 7:15–34, 2008.***

Alzheimer disease (AD)[1] is the most prevalent neurodegenerative disorder worldwide. A defining pathological hallmark of AD is the deposition of plaques, largely consisting of the 40–42-amino acid amyloid $\beta$-peptide (A$\beta$). A$\beta$ is generated by the consecutive cleavage of the amyloid precursor protein (APP) by two proteases, $\beta$-secretase and $\gamma$-secretase (1). Less than 10% of all AD cases are inherited. All mutations known to date that lead to early onset familial forms of AD occur either in APP itself or in protein components of the $\gamma$-secretase complex (2). Although a large body of literature exists that establishes the importance of a few key proteins for AD, our understanding of the cellular context in which these proteins operate is sketchy at best. It has, for example, long been hypothesized that APP represents a transmembrane receptor. However, despite the presence of a large and structurally complex extracellular domain within this protein, to this date no extracellular APP ligand has been firmly established as a physiological interactor. The significance of a recently reported *in vitro* interaction between F-spondin and a recombinant APP construct consisting of a conserved central extracellular domain of APP fused to GST remains to be established (3). Early studies suggested binding of APP to the intracellular GTP-binding protein $G_o$ (4). Various other intracellular interactions of APP, in particular with proteins (FE65, mDab1, X11$\alpha$, and Shc) that bear phosphotyrosine interaction domains, have been reported (5–7). Most of these phosphotyrosine interaction domain-mediated interactions involve an NP*X*Y motif present in the C-terminal domain of APP but are, somewhat surprisingly, observed to be independent of the phosphorylation status of the tyrosine within this motif (8). Following phosphorylation of FE65, a trimeric complex consisting of the APP intracellular domain (AICD), FE65 and the

From the [a]Centre for Research in Neurodegenerative Diseases and Departments of [d]Laboratory Medicine and Pathobiology, [h]Medical Biophysics, [k]Medicine (Neurology), University of Toronto, Ontario M5S 3H2, Canada, [g]New York University School of Medicine, Orangeburg, New York 10962, [j]Alberta Centre for Prions and Protein Folding Diseases, University of Alberta, Alberta T6G 2M8, Canada, and [l]Toronto Western Hospital Research Institute, Toronto Western Hospital, Toronto, Ontario M5S 3H2, Canada

Received, February 20, 2007, and in revised form, July 10, 2007

Published, MCP Papers in Press, October 13, 2007, DOI 10.1074/mcp.M700077-MCP200

[1] The abbreviations used are: AD, Alzheimer disease; A$\beta$, amyloid $\beta$-peptide; AICD, APP intracellular domain; APP, amyloid precursor protein; APLP1, amyloid precursor-like protein 1; APLP2, amyloid precursor-like protein 2; ER, endoplasmic reticulum; GPI, glycosylphosphatidylinositol; IP, immunoprecipitation; LINGO, LRR and Ig domain-containing, Nogo receptor interacting protein; LRR, leucine-rich repeat; tcTPC, time-controlled transcardiac perfusion cross-linking; TM, transmembrane; iTRAQ, isobaric tags for relative and absolute quantitation; PrP, prion protein; SCX, strong cation exchange; CHAPSO, 3-[(3-cholamidopropyl)dimethylammonio]-2-hydroxy-1-propanesulfonic acid; HEK, human embryonic kidney; APPsw, Swedish APP; siRNA, small interfering RNA; NCBI, National Center for Biotechnology Information; NCBInr, NCBI nonredundant database; NCAM, neural cell adhesion molecule; sAPP, soluble APP; EBP4.1, erythrocyte band 4.1 protein; ISH, *in situ* hybridization; $\alpha$CTF, $\alpha$-cleavage C-terminal fragment of APP; $\beta$CTF, $\beta$-cleavage C-terminal fragment of APP; GAP, GTPase-activating protein; SSC, saline sodium citrate; MEGAP, mental disorder-associated GTPase activating protein.

transcription factor CP2 (Tcfcp2) have been proposed to translocate to the nucleus and may regulate the expression of AICD-specific target genes (9). There also is literature that implicates APP in trafficking events. Initially it was reported that the cytoplasmic tail of APP binds to a microtubule-interacting protein, PAT1 (an acronym for protein interacting with APP tail 1), with sequence similarity to the light chain of the microtubule motor kinesin (10). Subsequent work then suggested binding of APP C-terminal sequences directly to kinesin-1 (11, 12) and proposed a causative relationship between this interaction and axonal swellings observed in a mouse model of Alzheimer disease (13). However, in a recent study involving independent laboratories, authors were unable to confirm the proposed direct interaction of APP and kinesin-1 (14). Recent work implicated the sorting protein-related receptor SorLa in the retrieval of APP from the membrane and documented genetic association of SorLa with Alzheimer disease (15, 16). It was further shown that paralogues of APP in Mammalia that include amyloid precursor-like protein 1 (APLP1) and amyloid precursor-like protein 2 (APLP2) can engage in heterodimerization with APP (17). In summary, there is no shortage of proposed interactors, but there is a lack of candidate interactors that enhance our understanding of molecular events that underlie assumed physiological functions of APP (18). As such, APP has been implicated in cellular activities ranging from cell adhesion and neuritogenesis to cell survival and homeostasis. The most informative studies conducted in target-specific knock-out animals support the prevalent view that APP contributes to events related to the formation of neuronal processes possibly in response to cellular damage (19–22). Although various scenarios can be invoked that implicate proposed interactors in such activities, a model is missing that more fully reconciles functional data with a molecular framework of protein-protein interactions. Contributing to this *status quo* are shortcomings of conventional strategies for the study of protein-protein interactions involving membrane proteins. Most approaches study membrane proteins outside their physiologic milieu or require them to be solubilized by detergents; however, how well a given membrane complex tolerates exposure to detergents is unpredictable.

Time-controlled transcardiac perfusion cross-linking (tcTPC) chemically links interacting proteins *in vivo* prior to the disruption of tissue integrity (23). It differs from standard perfusion fixation in that the cross-linking reagent is pumped through the circulatory system of the animal for only a short period of time, thereby allowing limited cross-linking to occur. As a result, tcTPC preserves physiological protein interactions and enables purification of protein complexes in the presence of high salt concentrations and detergents. These unique features of this protocol facilitate the downstream identification of cross-linked protein complex components by mass spectrometry.

In this report, we describe the application of tcTPC to study the molecular microenvironment of APP. Interactome maps were obtained following immunoprecipitation (IP) with antibodies that recognize non-overlapping epitopes of APP. To discriminate between APP-specific interactors and proteins that bind promiscuously to members of the APP family, we carried out comparative analyses of APP, APLP1, and APLP2 interactomes. Our data confirm previously reported interactions of APP with F-spondin, cystatin C, calsyntenin, calnexin, heat shock 70-kDa protein 5 (HSPA5, also known as BiP), prion protein (PrP), APLP1, and APLP2 and reveal more than 30 new protein interactions within the APP interactome. We demonstrate that the interactomes of APP, APLP1, and APLP2 are surprisingly different and demonstrate by quantitative and comparative iTRAQ analysis that this observation is not the result of sampling bias during LC/MS/MS analyses. Exemplary validation experiments on a novel APP candidate interactor, LINGO-1, confirm the interaction, demonstrate a strong correlation of APP and LINGO-1 expression in the brain, and suggest an important role for LINGO-1 in events that control the relative abundance of C-terminal APP fragments and secreted A$\beta$.

## EXPERIMENTAL PROCEDURES

*Antibodies*—The affinity-purified rabbit anti-APP intracellular domain antibody was raised against a synthetic peptide encompassing the terminal 45 amino acid residues of the APP cytoplasmic tail. The mouse monoclonal anti-APP extracellular domain antibody (clone mAmA3.2) was raised against the peptide antigen DAEFGHDSGFEVRHQC. Commercial rabbit antibodies specific for the C termini of APP (epitope MQQNGYENPTYKFFEQMQN), APLP1 (epitope NPTYRFLEERP), or APLP2 (epitope NPTYKYLEQMQI) were obtained from Sigma-Aldrich and Calbiochem (24). The polyclonal LINGO-1-directed antibody was obtained from Upstate/Millipore (Billerica, MA). Monoclonal anti-FLAG and anti-A$\beta$ antibodies (6E10) were purchased from Sigma-Aldrich and Signet (Berkeley, CA), respectively.

*tcTPC*—Mice were anesthetized intraperitoneally with Nembutal (sodium pentobarbital), and 0.2 ml of 1000 units/ml heparin solution was also administered to prevent blood clotting. Each mouse was placed on a gridiron mounted on top of a metal container. Muscular parts of the front paws were clamped with hemostats to stretch out the forelimbs. The chest was cut open in a caudal to rostral direction to the sternum along the sides of the rib cage and secured with either hemostats or retractor forceps. The tip of the heart was secured with forceps and then carefully clamped across with a curved hemostat. A slit was cut into the left ventricle, recognizable by its lighter color, into which a 30-mm-long 20-gauge needle with barrel tip, clamped into place with a hemostat and Luer lock hub, was inserted. The left atrium was cut, and the animal was perfused with saline at 25 ml/min for 2 min to purge the blood vessels. The success of this procedure was confirmed by a loss of color in the liver and the blood vessels that flank the midline of the rib cage. The perfusion was switched to fixative solution at 25 ml/min, and cross-linking was carried out for 6 min with the absence of blood in the tail and a hardening of the limbs of the animal signaling a successful perfusion. After perfusion, the brain was rapidly removed from the skull, postfixed in cross-linking reagent for up to 15 min at room temperature, and immediately frozen by immersion in liquid nitrogen. To increase the throughput of the tcTPC perfusions to 10/h, individual perfusions were initiated every 6 min in a procedure that required the parallel operation of two peristaltic pumps.

*Purification of Cross-linked Complexes*—All steps were carried out at 4 °C. tcTPC-treated brains were pooled and homogenized with 30

strokes of 10 s each (PowerGen 120; Fischer Scientific) in 5 ml/brain homogenization buffer (50 mM $NH_4Cl$, 40 mM Tris, pH 8.0) supplemented with 1× Complete protease inhibitor mixture (Roche Applied Science). To ensure near quantitative extraction of membrane proteins, 25 ml/brain extraction buffer (20 mM NaCl, 0.6% deoxycholate, 0.6% Nonidet P-40, 20 mM Tris, pH 8.0) was added followed by a 5-min sonication in a water bath sonicator. Insoluble cellular debris were removed by a low speed centrifugation; the sample was dialyzed against 20 mM NaCl, 20 mM Tris, pH 8.0, and further cleared from insoluble material by high speed centrifugation (100,000 × *g* for 1 h); and then the supernatant was filtered through a 0.45-$\mu$m cartridge. To concentrate the dilute extract, samples were loaded onto self-packed Q-Sepharose HP (GE Healthcare) and eluted with a steep salt gradient. The eluate was dialyzed and adjusted to 100 mM NaCl, 1% Nonidet P-40, 20 mM Hepes, pH 7.3, and again centrifuged at 100,000 × *g* for 1 h. The cross-linked protein complexes were immunoaffinity-captured following covalent attachment of antibodies to chemically activated Affi-Gel 10 matrix (Bio-Rad). Alternatively antibodies used for large scale co-immunoprecipitations were cross-linked with 20 mM dimethyl pimelimidate to Protein A-agarose (Sigma-Aldrich) in the presence of 25 mM borax, pH 9.4, using standard procedures (30 min at room temperature). During immunocapture samples were agitated on a turning wheel for 24 h, washed extensively with 0.5 M NaCl, 0.05% SDS, 1% Nonidet P-40, 20 mM Hepes, pH 7.3, and then further washed with 10 mM $NH_4HCO_3$, pH 8.0. Proteins were eluted by a reduction in pH resulting from the addition of 0.2% trifluoroacetic acid, 20% acetonitrile.

*Protein Reduction, Alkylation, and Trypsinization*—Protein-containing fractions were denatured in 6 M urea, 20 mM $NH_4HCO_3$, pH 8.0, followed by reduction with 1 mM tris(2-carboxyethyl)phosphine for 30 min at 60 °C and alkylation with 2.5 mM 4-vinylpyridine for 1 h at room temperature in the dark. Samples were diluted 4-fold to ensure that the concentration of urea did not exceed 1.5 M. Tryptic digestion was initiated by the addition of 1% (w/w) of side chain-modified, tosylphenylalanyl chloromethyl ketone-treated porcine trypsin and was allowed to proceed at 37 °C for 6 h.

*iTRAQ Labeling*—Protein-containing fractions were denatured in 6 M urea, 20 mM $NH_4HCO_3$, pH 8.0, followed by reduction with 1 mM tris(2-carboxyethyl)phosphine for 20 min at 70 °C and alkylation with 2.5 mM methylmethanethiosulfonate for 1 h at room temperature in the dark. Following trypsinization, equal quantities of tryptic peptide mixtures were spiked with 1 pmol of synthetic [$Glu^1$]fibrinopeptide B (Sigma-Aldrich) to serve in the downstream analysis as an internal control for the efficiency of individual labeling reactions. Equal labeling with all four reagents was confirmed by equal intensities of 114:115:116:117 signature peaks upon forced fragmentation of the [$Glu^1$]fibrinopeptide B parent ion at 785. Any strong deviation from this ratio would have indicated problems with the labeling reaction or recovery of individual samples prior to the sample mixing step. Individual iTRAQ labeling reagents (Applied Biosystems, Foster City, CA) were reconstituted in ethanol, added to peptide mixtures derived from the tryptic digestion of IP eluates (control, iTRAQ114; APP, iTRAQ115; APLP1, iTRAQ116; APLP2, iTRAQ117) and incubated at room temperature in the dark for 1 h.

*Two-dimensional Liquid Chromatography*—Strong cation exchange (SCX) chromatography was used to achieve peptide fractionation of the complex digest mixture. Samples digested with trypsin were adjusted to 25% acetonitrile and acidified (pH 3.0) by 20-fold dilution in 25% acetonitrile, 20 mM $KH_2PO_4$, pH 3.0. HPLC was carried out using the Ultimate System (Dionex, Sunnyvale, CA) equipped with a microflow calibration cartridge, a Valco injection port, and a 180-nl volume UV cell. Separation was achieved on a self-packed 0.5 × 110-mm Luna SCX (Phenomenex, Torrance, CA) column at a flow rate of 18 $\mu$l/min with a steep salt gradient from 0 to 400 mM $NH_4Cl$ in 25% acetonitrile, 20 mM $KH_2PO_4$, pH 3.0. Fractions eluted from the SCX column were desalted with $C_{18}$ Empore (3M, Minneapolis, MN) stop and go extraction tips (25) and subsequently subjected to nanoflow reversed phase HPLC using the Ultimate LC system (Dionex, Sunnyvale, CA) equipped with a nanoflow calibration cartridge at a flow rate of 250 nl/min. Peptides were separated on a 75-$\mu$m-inner diameter self-packed column containing Proteo $C_{12}$ reversed phase matrix (Phenomenex) using a 100-min gradient from 2 to 34% acetonitrile in water with 0.1% (w/v) formic acid as the ion pairing agent.

*ESI-Q-TOF Mass Spectrometry Analysis*—The column effluent was coupled directly via a fused silica capillary transfer line to a QSTAR XL hybrid quadrupole/time-of-flight tandem mass spectrometer (Applied Biosystems; MDS Sciex, Concord, Ontario, Canada) equipped with a MicroIonSpray source. The progress of each LC/MS run was monitored by recording the total ion current as a function of time for ions in the *m/z* range 300–1800. At 5-s intervals through the gradient, a mass spectrum was acquired for 1 s followed by one CID acquisition of 4 s each on ions selected by preset parameters of the information-dependent acquisition method using nitrogen as the collision gas. Singly charged ions were excluded from CID selection. The collision energy was adjusted automatically for each CID spectrum using an empirically optimized formula that considers the charge state and *m/z* value of the precursor ion.

*Database Searches*—Peak lists for database searching were created using Mascot Distiller (Version 1, Matrix Science, London, UK). Searches were performed using designated MS/MS data interpretation algorithms within Protein Prospector (Version 4.21.3, University of California, San Francisco, CA) (26) and Mascot (Version 1.9, Matrix Science). Modifications considered were oxidation of methionine, phosphorylations of serine and threonine, N-terminal (pyro)Glu, and alkylation with 4-vinylpyridine. Searches further considered up to one missed cleavage and charge states ranging from +2 to +4. For a protein to be listed in the data tables it had to be identified by both search algorithms. In the few instances were only two peptides supported the identification of a protein, we required the underlying CID spectra to generate a Mascot score indicating a <5% probability that the match could be considered a random event (27) and further confirmed matches by the peptide sequence tag approach (28) and manual interpretation of spectra. As searches were carried out without species restriction the correct assignment of matches to mouse entries served as an additional internal control. All identifications were confirmed in repeat experiments done at a 2-fold lower scale. Please note that the vast majority of proteins were identified with Mascot scores of more than 100 thereby significantly exceeding thresholds conventionally applied for confident identifications. Further corroboration of APP interactome data was obtained from overlapping identifications obtained in co-IP experiments that utilized antibodies directed against non-overlapping domains of APP. The mass tolerance range between expected and observed masses used for database searches was ±150 ppm for MS peaks and ±0.15 Da for MS/MS fragment ions. These relatively large thresholds were used to capture more of the low intense peaks that frequently display broader distribution and thus are assigned with lower mass accuracy. Threshold levels were optimized based on LC/MS/MS datasets of tryptic digests of standard proteins. All samples were searched against the National Center for Biotechnology Information nonredundant database (NCBInr; release November 25, 2006) and a "decoy" database in which all entries of the above NCBI database had been inverted. With a view to provide a complete representation of the data, some weak assignments of CID spectra to peptides were included in supplemental data tables whenever strong CID spectra were also present that supported highly confident identifications of the respective proteins. The analysis of iTRAQ data was assisted by the software program ProQuant (Applied Biosystems; MDS Sciex). A feature of this software package was used to correct raw

iTRAQ ratios for impurity levels of individual reagent lots determined by the manufacturer. To counteract the problem of low spectral counts present in a subset of spectra we set an intensity threshold for the combined intensities of iTRAQ signature peaks (≥40) that needed to be surpassed by a CID spectrum for it to be included in the calculation of averages and standard deviations of a given protein.

*Co-immunoprecipitation*—Wild-type CD-1 mouse brains were homogenized in 50 mM Tris-HCl (pH 7.5) containing 1% CHAPSO, 150 mM NaCl, and protease inhibitor mixture (Sigma-Aldrich), hereafter referred to as Buffer A. Following incubation overnight with the primary antibody, immunocomplexes were captured by Protein A-agarose (Sigma-Aldrich) during a 2-h incubation step. Next beads were excessively washed with Buffer A, and bound proteins were eluted in denaturing Laemmli SDS gel loading buffer assisted by incubation at 95 °C for 10 min. Following SDS-PAGE separation on 4–20% Tris-glycine gels, proteins were electrophoretically transferred to PVDF membranes. For immunodetection Western blots were incubated overnight at 4 °C with primary antibodies and for 2 h at room temperature with horseradish peroxidase-conjugated secondary antibodies. Protein bands were visualized by ECL.

*In Situ Hybridization*—Sections (6 μm) of formalin-fixed, paraffin-embedded mouse brains were cut using an RNase-free blade, mounted on slides, and dried overnight at 63 °C. Paraffin was removed by incubation in xylene followed by rehydration through a graded series of ethanol. Sections were postfixed in 10% formalin for 20 min, rinsed three times with TBS, and then incubated in 200 mM HCl for 15 min to denature proteins. Following three rinses with TBS, sections were placed in 0.5% acetic anhydride (in 0.1 M Tris-HCl, pH 8) for 10 min. Slides were rinsed three times with TBS and then incubated with 20 μg/ml proteinase K (Invitrogen) in TBS containing 2 mM $CaCl_2$ for 20 min at 37 °C. Sections were rinsed three times with TBS and then incubated in TBS at 4 °C for 5 min to stop the digestion. The sections were then dehydrated through a graded series of ethanol, incubated in chloroform for 20 min, rehydrated through decreasing concentrations of ethanol, and then incubated in 2× saline sodium citrate (SSC) for 5 min. Sections were prehybridized with hybridization buffer (2× SSC, 10% dextran sulfate, 0.01% sheared salmon sperm DNA, 0.02% SDS, 50% formamide) for 1 h at 56 °C. For hybridization, digoxigenin-labeled RNA probes were diluted 1:200 to 1:400 in hybridization buffer, and 40 μl of probe was applied per slide. The slides were coverslipped, heated at 95 °C for 5 min, and then hybridized overnight at 56 °C. Coverslips were removed by incubating the slides in 2× SSC for 15 min. Non-hybridized probe was removed by digestion with 20 μg/ml RNase A (Fermentas) in 0.5 M NaCl, 10 mM Tris-HCl, pH 8.0, for 30 min at room temperature. Sections were rinsed in 2× SSC and then incubated in 50% formamide, 1× SSC for 1 h at 56 °C to remove unbound probe. Sections were washed twice with 1× SSC for 15 min and then rinsed with TBS. Slides were blocked in blocking buffer (1× Blocking Reagent (Roche Applied Science) diluted in 0.1 M maleic acid, 0.15 M NaCl, pH 7.5) for 30 min at room temperature. Anti-digoxigenin antibody conjugated to alkaline phosphatase (Roche Applied Science) was diluted 1:500 in blocking buffer and then applied to the sections for 1 h at room temperature. Following two 15-min rinses with TBS, sections were incubated with detection buffer (0.1 M NaCl, 0.1 M Tris-HCl, pH 9.5) for 15 min. The alkaline phosphate substrate nitro blue tetrazolium/5-bromo-4-chloro-3-indolyl phosphate was added, and color development was allowed to proceed overnight at room temperature in the dark.

*Overexpression and Knockdown Analyses*—Full-length human LINGO-1 cDNA (gi accession number 15029688) equipped with a C-terminal FLAG tag was cloned into the pcDNA3.1d-TOPO vector (Invitrogen). Following sequence verification by primer walking the eukaryotic expression vector was transiently transfected into a human HEK293 cell line that stably expresses Swedish APP (APPsw). Cells were grown in Dulbecco's modified Eagle's medium supplemented with 10% fetal bovine serum in the presence of 5% $CO_2$ at 37 °C. APP-derived C83 and C99 fragments were distinguished by their distinct molecular weight and by Western blotting with APP C terminus-directed antibodies (recognizing both C99 and C83) and 6E10 (recognizing only C99).

siRNA knockdown experiments of LINGO-1 were based on On-Target-Plus reagents (Dharmacon, Lafayette, CO) and the following siRNA pairs: Pair 1, GCUGGCGGCUCAACUUCAAUU (sense) and PUUGAAGUUGAGCCGCCAGCUU (antisense); Pair 2, ACACAAAG-CACAACAUCGAUU (sense) and UCGAUGUUGUGCUUUGUGUUU (antisense); Pair 3, GGACUUCCCUGAUGUGCUAUU (sense) and PU-AGCACAUCAGGGAAGUCCUU (antisense); and Pair 4, GAACAAGA-UCGUUAUCCUAUU (sense) and PUAGGAUAACGAUCUUGUU (antisense). The siControl Non-Targeting Pool (D-001810-10) was used as a negative control. All transfections used the transfection reagent Lipofectamine 2000 (Invitrogen) according to the instructions of the manufacturer.

*Aβ ELISA*—Aβ40 levels were measured as described previously by ELISA using 12–24-h conditioned APPsw HEK293 cell medium (29, 30).

*Quantitative RT-PCR*—RNA was extracted from cells using the RNeasy Plus Mini kit (Qiagen, Mississauga, Ontario, Canada) according to the manufacturer's instructions. First strand cDNA was synthesized from 2 μg of RNA using the StrataScript QPCR cDNA Synthesis kit (Stratagene, La Jolla, CA) according to the protocol provided with the kit. First strand cDNA was then diluted 1:5 with distilled water, and 5 μl (per reaction) was used in a 20-μl reaction volume of quantitative PCR with SYBR Premix Ex Taq (Perfect Real Time) (TaKaRa Bio Inc., Otsu, Japan) in an ABI 7500 Real-Time PCR System (Applied Biosystems) using β-actin-specific primer pairs (ACTB-F, 5′-AACTGGAAC-GGTGAAGGTGAC-3′; ACTB-R, 5′-CAACAATGTGCAATCAAAGTCC-3′) and two LRRN6a-specific primer pairs (LRRN6a-A-F (5′-CACCT-GCCCTCCTTCTACCA-3′) and LRRN6a-A-R (5′-TCGTCGGCTTTCA-ACTCCA-3′) and LRRN6a-B-F (5′-TGGGCTTCATCTCTTTCCTG-3′) and LRRN6a-B-R (5′-GTGCTTTGTGTTGCCCTTG-3′)). For the relative expression measure of LRRN6a, β-actin primers were used as an internal control. A standard comparative Ct method (ddCt method implemented in Sequence Detection Software version 1.3.1 (Applied Biosystems)) was used for the assessment of relative expression patterns compared with a calibration group (mock transfection).

## RESULTS

*APP Interactome Mapping by tcTPC Procedure with a C Terminus-directed Antibody*—25 CD-1 mice were perfused in the presence of 4% formaldehyde for 15 min at room temperature. Cross-linking was stopped by immersion of the dissected target tissue into liquid nitrogen. Upon homogenization of the tissue of interest, residual formaldehyde was quenched with ammonium chloride and removed by dialysis. Due to the large volume of brain extracts used, the IP step was preceded by a protein concentration step using strong anion exchange chromatography. Target protein complexes were isolated by immunoaffinity purification in the presence of high salt concentration (0.5 M NaCl) and detergent (1% Nonidet P-40, 0.5% deoxycholate). The affinity purification step used an affinity-purified, APP C terminus-directed antibody that was covalently coupled to Affi-Gel 10, a chemically activated agarose matrix, and was carried out alongside a mock purification using an unspecific rabbit antibody. The extracted proteins were denatured in urea, alkylated with 4-vinylpyri-

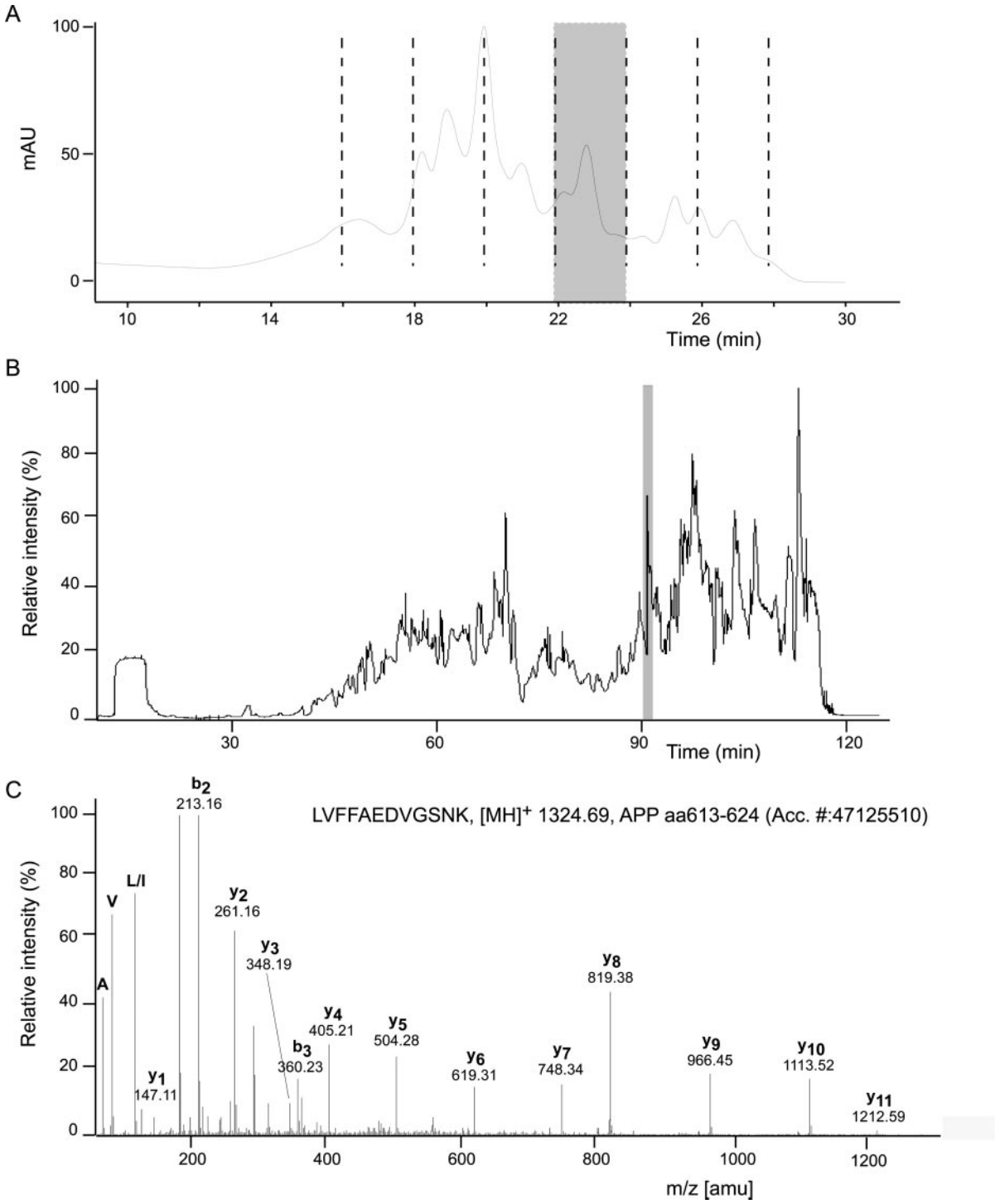


FIG. 1. **Identification of molecular neighbors of APP by a combination of *in vivo* cross-linking, affinity capture, proteolytic fragmentation, two-dimensional liquid chromatography, and mass spectrometry.** Mouse brains were subject to time-controlled transcardiac perfusion with formaldehyde to cross-link APP to its molecular neighbors. Complexes containing APP were then purified on an APP-specific immunoaffinity matrix. Following pH drop elution, captured proteins were trypsinized, and the complexity of the sample was reduced by two-dimensional liquid chromatography. *A*, UV trace from microbore HPLC strong cation exchange separation of trypsinized complexes containing APP. Six eluate samples were collected for subsequent capillary reversed phase HPLC separation and on-line ESI-MS/MS analysis. *B*, total ion current recorded during on-line reversed phase ESI-MS/MS analysis of representative cation exchange fraction indicated by the *shaded area* in *panel A*. *C*, representative CID spectrum generated from a $[M + 2H]^{2+}$ ion at *m/z* 662.835 ($[MH]^+$ 1324.69) which eluted from reversed phase column at time point indicated by the *shaded area* in *panel B*. In this spectrum the presence of both strong immonium ions in the low mass range and a continuous series of y-ions allowed high confidence assignment of the amino acid sequence (L/I)VFFAEDVGSNK, a tryptic peptide derived from APP. *mAU*, milliabsorbance units; *aa*, amino acids; *Acc*., accession.

TABLE I

*APP candidate interactors*

tcTPC of outbred mice followed by high stringency immunoaffinity purification and tandem mass spectrometry enabled identification of more than 30 protein components of APP-containing cross-linked complexes. Proteins are listed in order with the position of a given protein in the table reflecting the percentage of primary structure corresponding to the combined unique CID spectra. See supplemental Table 5 for proteins that were found in all specific and unspecific pulldowns and therefore represent unspecific binders to the affinity matrix.

| Identified proteins[a] | gi no. (NCBInr) | Molecular mass | Subcellular location[b] | A. Co-IP with C-terminal APP antibody[c] | | | B. Co-IP with extracellular APP antibody[c] | | |
|---|---|---|---|---|---|---|---|---|---|
| | | | | Peptide[d] | Unique[e] | Cov[f] | Peptide[d] | Unique[e] | Cov[f] |
| | | *kDa* | | | | % | | | % |
| **APP** | 47125510 | 87 | TM Type I | 27 | 59 | 46 | 40 | 95 | 60 |
| BiP protein, Grp78 (HSPA5) | 1304157 | 72 | ER | 29 | 37 | 45 | 32 | 47 | 50 |
| **Erythrocyte band 4.1-like 3 (EPB4.1l3)** | 7305031 | 103 | Inner PM | 34 | 63 | 44 | | | |
| **APLP2** | 1086521 | 87 | TM Type I | 16 | 29 | 29 | 6 | 15 | 10 |
| **Protein phosphatase I, inhibitor 2 (PPP1r2)** | 18859587 | 23 | Cytosol | 6 | 9 | 33 | | | |
| **Cystatin C (CYSC)** | 31981822 | 15 | Secreted | | | | 3 | 3 | 32 |
| **Thy-1 cell surface antigen (THY1)** | 6678347 | 13 | GPI | | | | 2 | 2 | 24 |
| **Contactin (CNTN1)** | 6680954 | 113 | GPI | | | | 17 | 18 | 21 |
| **APLP1** | 6680700 | 73 | TM Type I | 7 | 8 | 9 | 10 | 10 | 19 |
| Protein disulfide-isomerase A6 (PDIA6) | 60502437 | 49 | ER | 6 | 6 | 19 | | | |
| Cyclophilin B (PPIB) | 71774133 | 23 | ER | 3 | 3 | 18 | 2 | 2 | 13 |
| Calreticulin (CALR) | 50568 | 48 | ER | 3 | 3 | 12 | 5 | 6 | 15 |
| Calnexin (CALX) | 6671664 | 67 | ER | 5 | 7 | 11 | 7 | 8 | 16 |
| Calumenin (Calu) | 6680840 | 37 | ER | 3 | 3 | 15 | | | |
| **Oat protein (OAT)** | 8393866 | 48 | Mito. matrix | | | | 4 | 4 | 14 |
| ***S*-Adenosylmethionine synthetase (MAT1a)** | 21704144 | 44 | Cytosol | 4 | 4 | 14 | | | |
| GRP94 (HSP90b1) | 6755863 | 83 | ER | 4 | 4 | 7 | 5 | 5 | 12 |
| **Extracellular matrix protein 2 (SPARl1)** | 1498641 | 72 | Secreted | 3 | 3 | 4 | 5 | 6 | 10 |
| **F-spondin (SPON1)** | 21704174 | 82 | Secreted | | | | 6 | 6 | 10 |
| Reticulocalbin 2 (RCN2) | 6755302 | 37 | ER | 5 | 5 | 13 | | | |
| **Carboxypeptidase E (CPE)** | 22203763 | 53 | Secreted | | | | 3 | 4 | 9 |
| **PrP** | 200527 | 28 | GPI | | | | 2 | 2 | 9 |
| **NCAM1** | 15030115 | 119 | TM Type I | | | | 7 | 7 | 7 |
| **LINGO-1, alias LRRN6a (LRRN6a)** | 30841016 | 70 | TM Type I | | | | 3 | 4 | 7 |
| **MEGAP, srGAP3 (SRGAP3)** | 48428625 | 124 | Inner PM | 5 | 5 | 7 | | | |
| **Plasma membrane calcium ATPase 2 (ATP2b2)** | 6753140 | 133 | TM Type III | 2 | 2 | 2 | 5 | 5 | 6 |
| Thioredoxin domain-containing 4 (TXNDC4) | 19072792 | 47 | ER | 2 | 2 | 6 | | | |
| GRP170 (HYOU1) | 31542333 | 111 | ER | | | | 4 | 5 | 4 |
| **GABA-B1a receptor (GABBR1)** | 4544337 | 108 | TM Type III | 2 | 2 | 2 | 3 | 3 | 3 |
| **Neurofascin (NFASC)** | 35215309 | 138 | TM | | | | 3 | 3 | 3 |
| Neutral $\alpha$-glucosidase AB (GANAB) | 38371758 | 107 | ER | | | | 3 | 3 | 3 |
| **Calsyntenin 3 (CLSTN3)** | 13162190 | 109 | TM Type I | 2 | 2 | 3 | | | |
| **Calsyntenin 1 (CLSTN1)** | 12746426 | 109 | TM Type I | 2 | 2 | 4 | 5 | 6 | 2 |
| Heat shock 70-kDa protein 4 (HSPA4) | 38327083 | 94 | ER | 6 | 6 | 11 | | | |

[a] In instances where a subset of CID spectra were matched to more than one isoform or member of a protein family only the highest scoring entry was selected unless an independent identification was supported by at least two unique CID spectra. Proteins APP is likely to encounter outside the secretory pathway are shown in bold.

[b] Only predominant physiological locations of proteins are indicated. PM, plasma membrane; Mito., mitochondrial.

[c] Only CID spectra were considered for which no higher ranked assignment to other proteins could be made in a search with a precursor ion mass tolerance of 150 ppm, a fragment ion mass accuracy of 0.15 Da, and no species restriction. Please refer to Supplemental Table 1 for more information on peptide sequences that underlie individual protein identifications.

[d] Only CID spectra underlying different peptides were considered, *i.e.* if the same peptide was identified with different charge states or modifications it counted as one hit.

[e] Total number of unique CID spectra. Please note that the same peptide was only counted more than once if it was identified with different charge states or modifications.

[f] Percent sequence coverage based on the presence on peptides for which no higher ranked assignment to other proteins could be made.

dine, and digested with trypsin. Resulting peptides were resolved on a strong cation exchange matrix into six fractions (Fig. 1*A*), which subsequently were subjected to on-line LC/MS/MS analysis (Fig. 1, *B* and *C*). A computational search of the non-redundant database at the National Center for Biotechnology Information (release November 25, 2006) with masses extracted from CID spectra identified candidate proteins cross-linked to C-terminal APP fragments during tcTPC. Searches against a "decoy database" in which all sequence entries of the above NCBI database were inverted did not give rise to any protein identification that passed significance thresholds we had applied, *i.e.* although searches of the decoy database indicated a low false positive rate with which CID spectra were assigned to individual peptides (with the

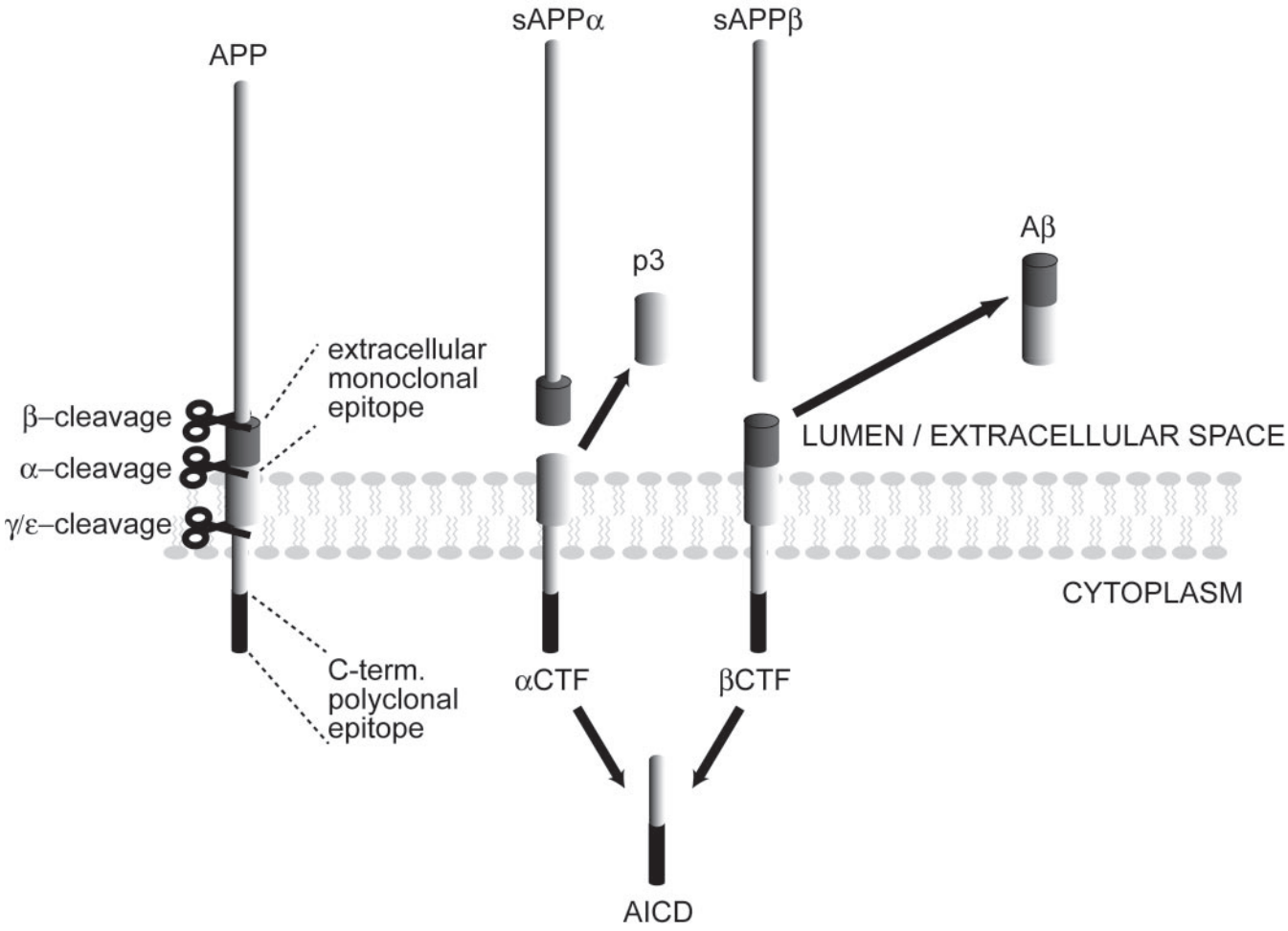


FIG. 2. **Schematic depiction of prominent biological fragments of APP and their detection with antibodies used for immunocapture in this work.** It is generally assumed that alternative extracellular cleavages of APP with α- and β-secretases are responsible for the release of sAPPα and sAPPβ fragments, respectively. The concomitantly generated αCTF and βCTF remain bound to the membrane and can subsequently be further truncated by ε/γ-secretase cleavage activities. The latter intramembrane proteolytic events cause the release of the AICD into the cytosol and the shedding of P3 (derived from αCTF) or Aβ fragments (derived from βCTF) into the luminal/extracellular space. APP epitopes of the extracellular domain-directed monoclonal and the C terminus-directed polyclonal antibodies are indicated in this figure in *dark gray shading* and *black*, respectively.

strongest assignment achieving a Mascot score as high as 59), in no instance could more than one CID spectrum be assigned to the same protein entry in the decoy database, and none of the false positive peptide assignments belonged to a mouse protein. The immunoaffinity purification was repeated once, and only proteins were considered that consistently co-purified with the bait (Table I, part A). The identification of each of these proteins relied on strong CID spectra from at least two peptides. In fact, for each of the 20 most abundant proteins, more than 10% sequence coverage was recorded, and the strongest identifications were based on more than 50 unique CID spectra and 40% sequence coverage. A representative CID spectrum showing a continuous y-ion series spanning the entire tryptic peptide sequence LVFFAEDVGSNK contributed to the identification of APP as the most prominent component of these cross-linked complexes (Fig. 1*C*). Other nonspecific components were also present in eluate samples from this immunoaffinity purification as described below.

*APP Interactome Mapping by tcTPC Procedure with Antibody Recognizing Extracellular Domain of APP*—To facilitate the discrimination of specific *versus* nonspecific interactors, obtain better coverage of the heterogeneous APP molecule population, and overcome steric constraints for cross-linking and antibody recognition, the APP-directed tcTPC study was repeated, following the experimental strategy outlined above, with a different immunoaffinity matrix. Instead of utilizing C terminus-directed antibodies, the second approach relied on a monoclonal antibody directed against an extracellular domain of APP that is flanked by α- and β-secretase cleavage sites and therefore recognizes full-length APP and soluble APPα but has no cross-reactivity to APLP1 or APLP2 (Fig. 2).

TABLE II
*APLP1 candidate interactors*

Please refer to supplemental Table 2 for more information on peptide sequences that underlie individual protein identifications.

| Identified proteins[a] | gi no. (NCBInr) | Molecular mass | Subcellular location[b] | CID spectra[c] | | |
|---|---|---|---|---|---|---|
| | | | | Peptides[d] | Unique[e] | Cov[f] |
| | | *kDa* | | | | % |
| **APLP1** | 6680700 | 73 | TM Type I | 32 | 39 | 53 |
| **RasGAP-activating-like protein 1 (RASAL1)** | 31980729 | 89 | Inner PM | 16 | 17 | 31 |
| **Unnamed protein product (BNIPXL$\alpha$ ?)** | 26332961 | 38 | ? | 6 | 6 | 27 |
| **Phosphatidic acid phosphatase 2c (PPAP2c)** | 16307571 | 31 | Inner PM | 3 | 4 | 16 |
| **Neurosecretory protein VGF (VGF8a)** | 82899660 | 62 | Synapses | 7 | 8 | 15 |
| **APP** | 47125510 | 87 | TM Type I | 7 | 7 | 13 |
| **Phosphatidic acid phosphatase 2a (PPAP2a)** | 6679431 | 32 | Inner PM | 2 | 3 | 7 |

[a] In instances where a subset of CID spectra were matched to more than one isoform or member of a protein family only the highest scoring entry was selected unless an independent identification was supported by at least two unique CID spectra. Proteins APLP1 is likely to encounter outside the secretory pathway are shown in bold.

[b] Only predominant physiological locations of proteins are indicated. PM, plasma membrane.

[c] Only CID spectra were considered for which no higher ranked assignment to other proteins could be made in a search with a precursor ion mass tolerance of 150 ppm, a fragment ion mass accuracy of 0.15 Da, and no species restriction. Please refer to Supplemental Table 1 for more information on peptide sequences that underlie individual protein identifications.

[d] Only CID spectra underlying different peptides were considered, *i.e.* if the same peptide was identified with different charge states or modifications it counted as one hit.

[e] Total number of unique CID spectra. Please note that the same peptide was only counted more than once if it was identified with different charge states or modifications.

[f] Percent sequence coverage based on the presence on peptides for which no higher ranked assignment to other proteins could be made.

Also in this second Co-IP experiment the chemically activated agarose matrix was replaced with Protein A-agarose beads, and the antibody was covalently stabilized with the homobifunctional cross-linker dimethyl pimelimidate. As seen with the C terminus-directed APP antibody, this APP-specific dataset again was highly enriched in proteins that have been implicated in processes related to endoplasmic reticulum (ER) folding and quality control. Interestingly despite the fact that this antibody should not cross-react with APLP1 or APLP2, both proteins presented in the dataset with strong protein identification data. Consistent with the notion that the monoclonal antibody recognizes APP gene products retaining an extracellular domain (Fig. 2) and therefore will, following *in vivo* cross-linking, primarily shed light on extracellular binding partners of APP, this second dataset contained various additional proteins that are known to localize to the extracellular space (F-spondin and Sparc-like protein-1) or are anchored in the plasma membrane with either a single transmembrane domain (neurofascin, neural cell adhesion molecule 1 (NCAM1), and LINGO-1) or a glycosylphosphatidylinositol (GPI) anchor (contactin, NCAM1-GPI, Thy-1, and PrP) (Table I, part B). In all, 12 APP candidate interactors were shared among the two subdatasets, and 10 proteins each were exclusively identified in protein lists associated with the individual antibodies.

*Applying tcTPC to APP Family Members APLP1 and APLP2*—To further refine the list of APP-specific interactors we extended tcTPC-based interactome mapping experiments to APLP1 and APLP2. The direct comparison of interactome datasets thus obtained was to facilitate discrimination of member-specific and group-specific interactions. APLP1- and APLP2-specific antibodies used for immunoaffinity purification of tcTPC-derived extracts had been raised against short C-terminal peptides and shown to not cross-react with other APP family members (24). Downstream sample processing and analysis followed the steps outlined above for APP and resulted in the identification of distinct candidate interactors of APLP1 (Table II) and APLP2 (Table III). As above, the identification of each protein was based on obtaining strong and unique CID spectra from at least two peptides.

The combined analysis of interactome data collected enabled sorting of proteins into three groups. The first group contains nonspecific binders to the affinity matrix found in all eluates, including mock eluates (supplemental Table 5). This group largely consisted of abundant cellular proteins such as cytosolic actin and tubulin, glycolytic enzymes, and components of the electron transport chain that are localized to the inner mitochondrial membrane. The second group contains interactors unique to APP (Table I), APLP1 (Table II), or APLP2 IP (Table III). The third group comprises proteins found in more than one specific co-immunoprecipitation, *i.e.* the APP-, APLP1-, and APLP2-directed IPs but not seen in mock IP eluates. To our surprise, the latter group was very small and, aside from the occurrence of the small RasGAP-activating-like protein 1 found in both APLP1 and APLP2 interactomes, only revealed mutual interactions of APP family member proteins with each other. Taken together, these data provide a comprehensive network of proteins that interact directly or indirectly with APP and its mammalian homologues (Fig. 3; see also supplemental Tables 1–3). All proteins incorporated in this network were identified with high fidelity based on at least two unique and manually confirmed tandem MS spectra.

TABLE III
*APLP2 candidate interactors*

Please refer to supplemental Table 3 for more information on peptide sequences that underlie individual protein identifications.

| Identified proteins[a] | gi no. (NCBInr) | Molecular mass | Subcellular location[b] | CID spectra[c] | | |
|---|---|---|---|---|---|---|
| | | | | Peptides[d] | Unique[e] | Cov[f] |
| | | *kDa* | | | | % |
| **APLP2** | 1086521 | 87 | TM Type I | 30 | 59 | 52 |
| **Growth arrest-specific 7-cb (GAS7-cb)** | 6531399 | 40 | Cytosol | 8 | 12 | 28 |
| **Kinesin family member 1A (KIF1a)** | 6680558 | 192 | Cytosol | 32 | 39 | 25 |
| **Retinitis pigmentosa 2 homolog (RP2h)** | 19526820 | 39 | Cytosol | 7 | 9 | 22 |
| **Ras-related C3 botulinum substrate 1 (RAC1)** | 12842616 | 23 | Cytosol | 4 | 4 | 21 |
| **Protein phosphatase type 2A (PP2ac)** | 3342500 | 36 | Cytosol | 4 | 4 | 19 |
| **RasGAP-activating-like protein 1 (RASAL1)** | 4185296 | 89 | Cytosol | 8 | 10 | 16 |
| **Copine 8 (CPNE8)** | 21630253 | 65 | Cytosol | 6 | 7 | 16 |
| **Rho family GTPase (RHOA)** | 3237320 | 22 | Cytosol | 2 | 3 | 13 |
| **APP** | 47271504 | 78 | TM Type I | 8 | 11 | 12 |

[a] In instances where a subset of CID spectra were matched to more than one isoform or member of a protein family only the highest scoring entry was selected unless an independent identification was supported by at least two unique CID spectra. Proteins APLP2 is likely to encounter outside the secretory pathway are shown in bold.

[b] Only predominant physiological locations of proteins are indicated.

[c] Only CID spectra were considered for which no higher ranked assignment to other proteins could be made in a search with a precursor ion mass tolerance of 150 ppm, a fragment ion mass accuracy of 0.15 Da, and no species restriction. Please refer to Supplemental Table 1 for more information on peptide sequences that underlie individual protein identifications.

[d] Only CID spectra underlying different peptides were considered, *i.e.* if the same peptide was identified with different charge states or modifications it counted as one hit.

[e] Total number of unique CID spectra. Please note that the same peptide was only counted more than once if it was identified with different charge states or modifications.

[f] Percent sequence coverage based on the presence on peptides for which no higher ranked assignment to other proteins could be made.

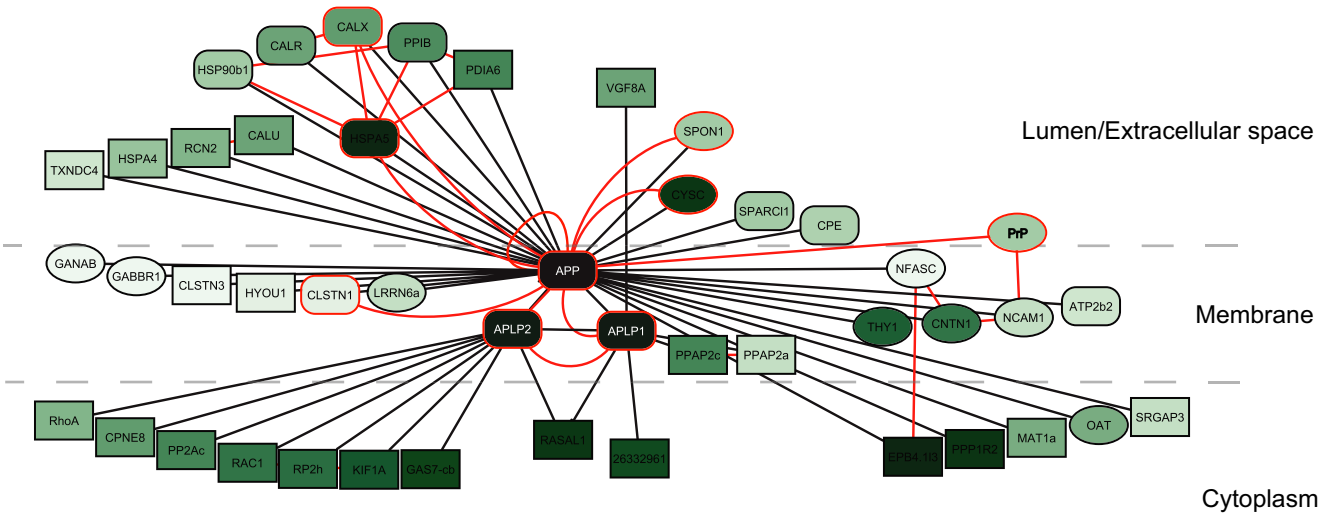


FIG. 3. **The APP protein family interactome.** The schematic shows components of the APP interactome as *nodes* and their direct or indirect interactions as *edges* in this network. APP family members used as baits for co-immunoaffinity purification of cross-linked interactors are shown with *white letters*. Components identified in previous studies by other investigators are shown with *red lines surrounding* and *red edges connecting* the nodes. The latter interactions were found in Bind and DIP (dip.doe-mbi.ucla.edu) protein interaction databases accessed through the Cytoscape platform or identified by querying the PubMed reference library (www.ncbi.nlm.nih.gov/entrez/query.fcgi?DB=pubmed). The intensity of the *green* fill color for the nodes indicates the fractional sequence coverage with which individual components of this network were identified by tandem mass spectrometry, *i.e.* the *darker* the *green* color the greater the sequence coverage underlying the protein identification. Finally the shape of the nodes indicates whether a protein was identified in co-immunopurifications using an antibody directed against the C terminus (*rectangular shape*), the extracellular domain (*oval shape*), or both (*rectangular* with *rounded corners*) of the APP family member bait protein. For abbreviations of protein names please see Tables 1–3.

A

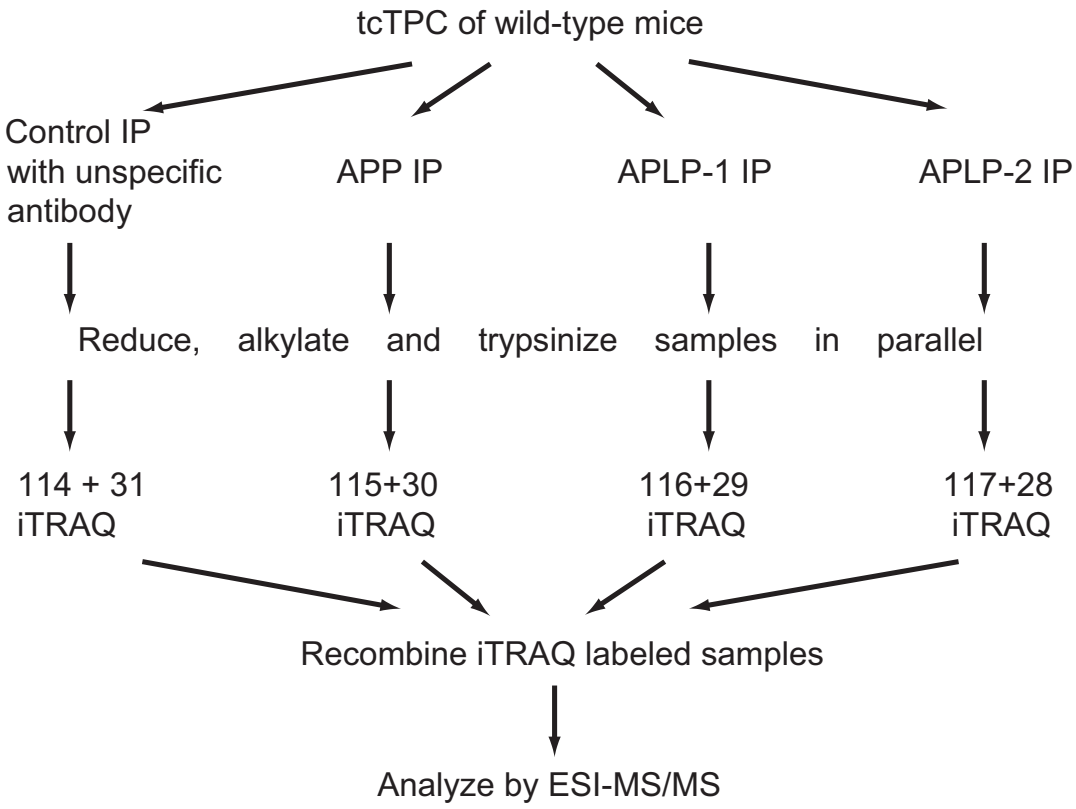


B TFAPEEISAMVLTK + iTRAQ(K) +iTRAQ114(N-term), $[MH]^+$ 1825.00, BiP aa140-153 (Acc. #:1304156)

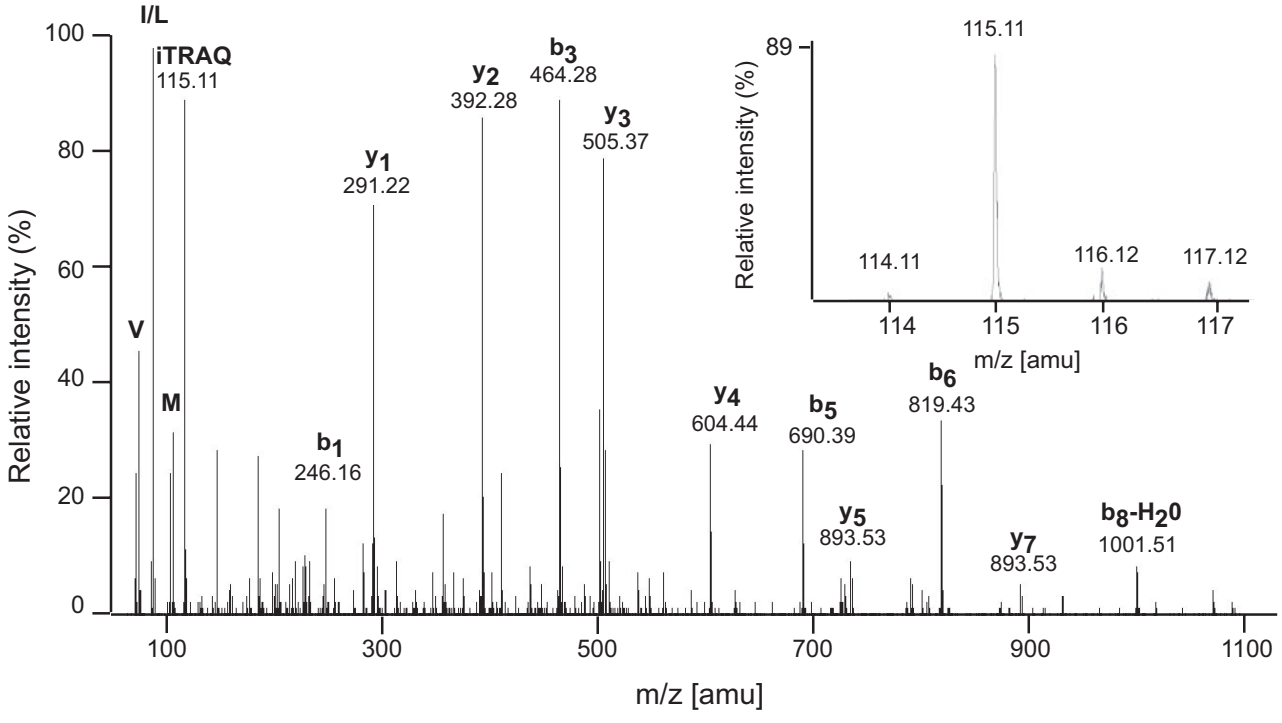

Multiple factors may contribute to the sequence coverage with which a protein is represented in such a cross-linking dataset. Proteins for which higher sequence coverage was obtained (indicated with *increasingly dark green shading* of network nodes) may *e.g.* engage in strong, persistent interactions with the bait proteins or may merely provide better access for the cross-link reagent to functional groups that support the generation of cross-links. It is to be expected that weak, temporary, or spatially restricted interactions are represented with less sequence coverage or missed altogether. In particular, short lived interactions of catalytic nature (*e.g.* proteolytic enzymes) commonly escape detection following chemical cross-linking and as a result may not be found in this network. Seven of 45 proteins present in this network, *i.e.* 15% of the identified proteins (depicted with *node boundaries* in *red*), had previously been reported to interact with APP. Strikingly many of the proteins we identified are, as expected for APP-interacting proteins, either directly embedded in membranes or are known to reside in close proximity to the plasma membrane. Please note that levels of soluble APP (sAPP) in mouse brains exceed levels of the APP holoprotein by a factor of 4.[2] In agreement with the notion that a large proportion of APP family proteins are subjected to proteolytic cleavage at sites near or within their transmembrane domains relatively early during their passage through the secretory pathway, antibodies directed against intracellular domains of the bait proteins largely identified proteins that are known to reside in the cytoplasm (depicted with *rectangular nodes*). In contrast, the antibody directed against the extracellular domain of APP predominantly contributed interactors to this network (depicted with *oval nodes*) that are known to reside extracellularly. Finally proteins identified by both intracellular and extracellular domain-directed antibodies (shown with *rounded-edge rectangular nodes*) are either known to be embedded in the membrane themselves, consistent with the notion that they may contribute domains for cross-linking to both intracellular and extracellular domains of APP, or are known to reside in the ER, a compartment to which APP is expected to transit at a time in its cellular life cycle at which it has not yet been subjected to proteolytic cleavage events.

A closer look at the network revealed APP residing in close proximity to both GPI-anchored contactin and intracellular membrane-associated erythrocyte band 4.1 protein (EBP4.1), proteins that repeatedly have been shown to constitute a well described protein complex known to also harbor the membrane-spanning contactin-associated protein. Strikingly, however, EBP4.1 and contactin were not identified in the same co-immunoprecipitation experiment but gave rise to strong identifications (based on 63 and 18 unique CID spectra for EBP4.1 and contactin, respectively) in independent immunoprecipitations using intracellular or extracellular antibodies directed against APP. This segregation of the proteins in the two subdatasets suggested cross-linking of intracellular and extracellular fragments rather than full-length APP to EBP4.1 and contactin, respectively, and thereby is consistent with the localization of the latter proteins with respect to the membrane. More importantly, the absence of contactin-associated protein-derived peptides from both datasets demonstrated the stringency of the washing steps we used and suggested that contamination of this network with proteins that were indirectly bound or cross-linked to the bait proteins may not be a major factor.

*iTRAQ-based Semiquantitative Analysis of APP, APLP1, and APLP2 Interactomes Confirms Specificity of Interactions*—Mass spectrometry is not a quantitative analytical tool *per se* and in particular for complex samples is known to suffer from run-to-run variance. It can then be argued that differences in lists of candidate interactors may not reflect differences in physiologically relevant interactomes but are a consequence of sampling bias during LC/MS/MS analyses (31–33). To address this possibility mouse brains were subjected to the tcTPC procedure, and material for subsequent IPs was prepared as described above. The material was split into four equal volumes, and parallel IPs were carried out with equal quantities of mock IgG and C-terminal antibodies directed against APP, APLP1, and APLP2. Immunoaffinity eluates from the individual precipitations were reduced, alkylated, trypsinized, and labeled with iTRAQ reagents 114–117 (mock, iTRAQ114; APP, iTRAQ115; APLP1, iTRAQ116; APLP2, iTRAQ117). Following the labeling reaction the four samples were combined, the peptide mixture was fractionated by strong cation exchange, and individual fractions were analyzed by LC/MS/MS as described above (Fig. 4*A*). For computational protein identification the presence of iTRAQ adducts at the N terminus of peptides and in positions of lysine, arginine, and histidine were considered. The relative

[2] P. Mathews, personal communication.

FIG. 4. **Semiquantitative comparison of interactomes of APP, APLP1, and APLP2 confirms preferential binding of BiP to APP.** *A*, schematic representation of the strategy for quantitative and comparative analysis of APP family member interactomes. The formaldehyde cross-linking solution is pumped through the circulatory system of the mouse in a parameter-defined manner. Cross-linked protein complexes are stringently purified with target-specific antibodies recognizing the C termini of APP family members followed by alkylation and trypsinization. Digests from mock, APP, APLP1, and APLP2 affinity purifications are side-by-side iTRAQ-labeled and subsequently combined. Two-dimensional liquid chromatography of peptides is coupled to on-line ESI-MS/MS, which is followed by computationally aided protein identification and quantitation. *B*, BiP-derived peptide is specifically found in APP IP. Parallel co-IPs from wild-type mouse brain extract were followed by trypsinization of eluates and parallel iTRAQ labeling of peptides. iTRAQ labeling reactions were set up as indicated above, *i.e.* iTRAQ114 label, control antibody; iTRAQ115 label, APP; iTRAQ116 label, APLP1; and iTRAQ117 label, APLP2. *Inset*, high resolution graph depicting iTRAQ signature mass peaks. For information on additional peptides see supplemental Table 4. *aa*, amino acids.

TABLE IV

*Quantitative comparison of interactomes confirmed selective binding of BiP to APP but not to APLP1 or APLP2*

Please refer to supplemental Fig. 1 for additional sample spectra and to supplemental Table 4 for Mascot scores and more information on peptide sequences that underlie individual protein identifications.

| Identified proteins[a] | gi no. (NCBInr) | Molecular mass | Peptides[b] | Unique[c] | Cov[d] | IPs and iTRAQ[e] | | | |
|---|---|---|---|---|---|---|---|---|---|
| | | | | | | 114 Control | 115 APP | 116 APLP1 | 117 APLP2I |
| | | *kDa* | | | % | | | | |
| Specific binders | | | | | | | | | |
| APP | 47125509 | 87 | 20 | 28 | 33 | 3.3 | 83.1 | 7.7 | 5.9 |
| BiP protein (HSPA5) | 1304156 | 72 | 19 | 20 | 32 | 4.4 | 78.8 | 9.1 | 7.8 |
| APLP2 | 1086521 | 87 | 19 | 20 | 29 | 3.1 | 24.4 | 7.5 | 65.0 |
| APLP1 | 6680700 | 73 | 15 | 19 | 25 | 2.4 | 10.1 | 79.1 | 8.4 |
| Unspecific binders | | | | | | | | | |
| Tubulin $\alpha$ -1 (TUBA1) | 6755901 | 50 | 7 | 7 | 25 | 14.6 | 27.0 | 28.8 | 29.5 |
| Tubulin $\beta$ -2 (TUBB2A) | 13542680 | 50 | 12 | 16 | 45 | 14.9 | 27.2 | 27.6 | 30.3 |
| 14-3-3 $\gamma$ (YWHAG) | 74215924 | 28 | 8 | 9 | 23 | 24.2 | 30.0 | 23.7 | 22.1 |

[a] In instances where a subset of CID spectra were matched to more than one isoform or member of a protein family only the highest scoring entry was selected unless an independent identification was supported by at least two unique CID spectra. Proteins were sorted into specific *versus* unspecific binder categories based on their iTRAQ distribution, *i.e.* proteins were considered unspecific interactors if their derived CID spectra revealed iTRAQ114–117 signature mass peak signal intensities that exceeded 10% of combined intensities for all samples including the unspecific control.

[b] Only CID spectra underlying different peptides were considered, *i.e.* if the same peptide was identified with different charge states or modifications it counted as one hit.

[c] Total number of unique CID spectra. Please note that the same peptide was only counted more than once if it was identified with different charge states or modifications.

[d] Percent sequence coverage based on the presence on peptides for which no higher ranked assignment to other proteins could be made.

[e] For the calculation of iTRAQ values the intensity of individual peptide-associated iTRAQ signature peaks was normalized to combine to 100% per peptide and subsequently averaged. Standard deviations were determined and are listed in supplemental Table 4.

contribution of individual samples to the abundance of a given peptide was derived from the relative abundance of iTRAQ reporter group peaks at *m/z* of 114, 115, 116, and 117 in the CID spectrum. The relative quantity of individual proteins across the four samples was then determined by averaging the abundance ratios of thus quantified peptides (Table IV; see also supplemental Table 4).

As the total amount of starting material was considerably lower in this experiment than in IPs described above, the computational data analysis revealed the identities of fewer target-specific proteins. Also not surprisingly we observed a bias toward the identification and subsequent quantitation of peptides found in more than one sample. Underlying this bias is the isobaric nature of the four iTRAQ reagents that translates into cumulative intensities of parent ions derived from proteins that bind unspecifically to affinity matrices or represent general contaminants of IP samples. However, consistent with the experimental setup, peptides derived from either APP (*e.g.* CLVGEFVSDALLVPDL) or its mammalian homolog APLP1 (*e.g.* SWPLGGR) were in this experiment primarily found in fractions labeled with the corresponding iTRAQ115 and iTRAQ116 reagents, respectively (supplemental Fig. 1, *A* and *B*). Our iTRAQ data further substantiated the view that a subset of cellular chaperones such as BiP, which is known to assist folding of nascent proteins during their passage through the secretory pathway, primarily cross-link to APP and are only weakly represented in APLP1 or APLP2 cross-link samples (Fig. 4*B*). Similarly a protein such as the erythrocyte band 4.1-like 3 protein, which we initially identified exclusively in the APP-derived dataset (Table I), here gave rise to strong iTRAQ115 signals but was absent from the APLP1 and APLP2 datasets (supplemental Fig. 1C and supplemental Table 4). This sample specificity of individual proteins contrasts the relative even distribution (indicated by similar iTRAQ114–117 average signals) of proteins such as tubulin (supplemental Fig. 1D) or 14-3-3 proteins that we routinely observe as unspecific contaminants in IP samples. In summary, the iTRAQ data presented here are in excellent agreement with data obtained following analysis of individual IPs (Tables I–III) and as such strongly argue that mere sampling bias was not the underlying cause for differences seen above in interactome data of APP protein family members.

*Validation of LINGO-1 as a Physiological Interactor of APP*—To establish the biological significance of novel interactions revealed in this work we focused on LINGO-1, alias LRRN6a, a transmembrane protein that intriguingly was reported to bind to p75, a receptor that, just like APP, represents a substrate for intramembrane proteolytic cleavages mediated by the $\gamma$-secretase complex. Our interest in a possible interaction of LINGO-1 and APP was further sparked by the strong association of LINGO-1 with processes related to the myelination and regeneration of axons, both activities that also feature prominently in the APP literature. To assess the benefit of cross-linking for the detection of LINGO-1 and validate the biochemical interaction between APP and LINGO-1 we carried out a series of co-IP experiments with

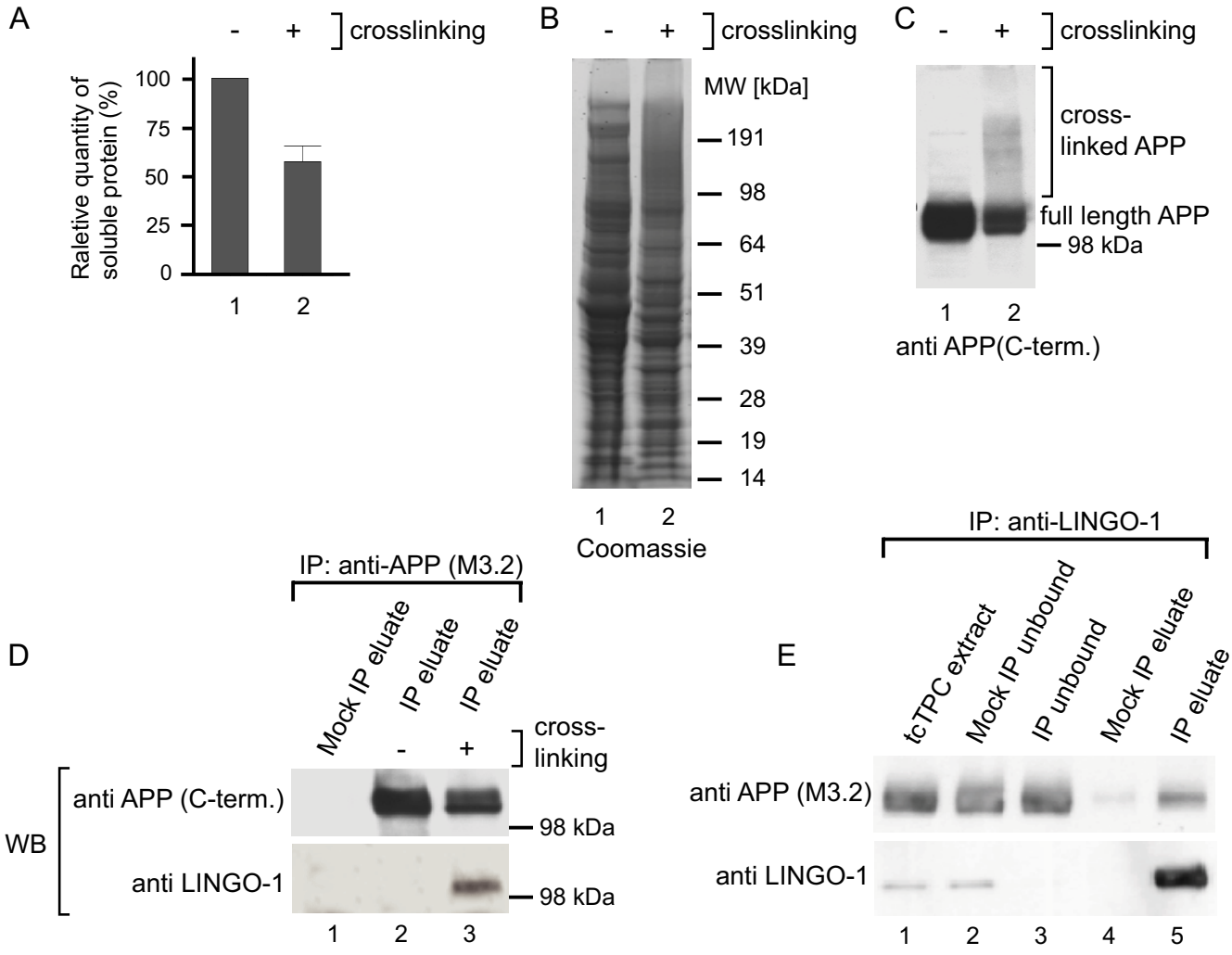
A
- + crosslinking
Raletive quantity of soluble protein (%)
100
75
50
25
0
1 2
B
- + crosslinking
MW [kDa]
191
98
64
51
39
28
19
14
1 2
Coomassie
C
- + crosslinking
cross-linked APP
full length APP
98 kDa
1 2
anti APP(C-term.)
D
IP: anti-APP (M3.2)
Mock IP eluate
IP eluate
IP eluate
- +
cross-linking
WB
anti APP (C-term.)
anti LINGO-1
98 kDa
98 kDa
1 2 3
E
IP: anti-LINGO-1
tcTPC extract
Mock IP unbound
IP unbound
Mock IP eluate
IP eluate
anti APP (M3.2)
anti LINGO-1
1 2 3 4 5

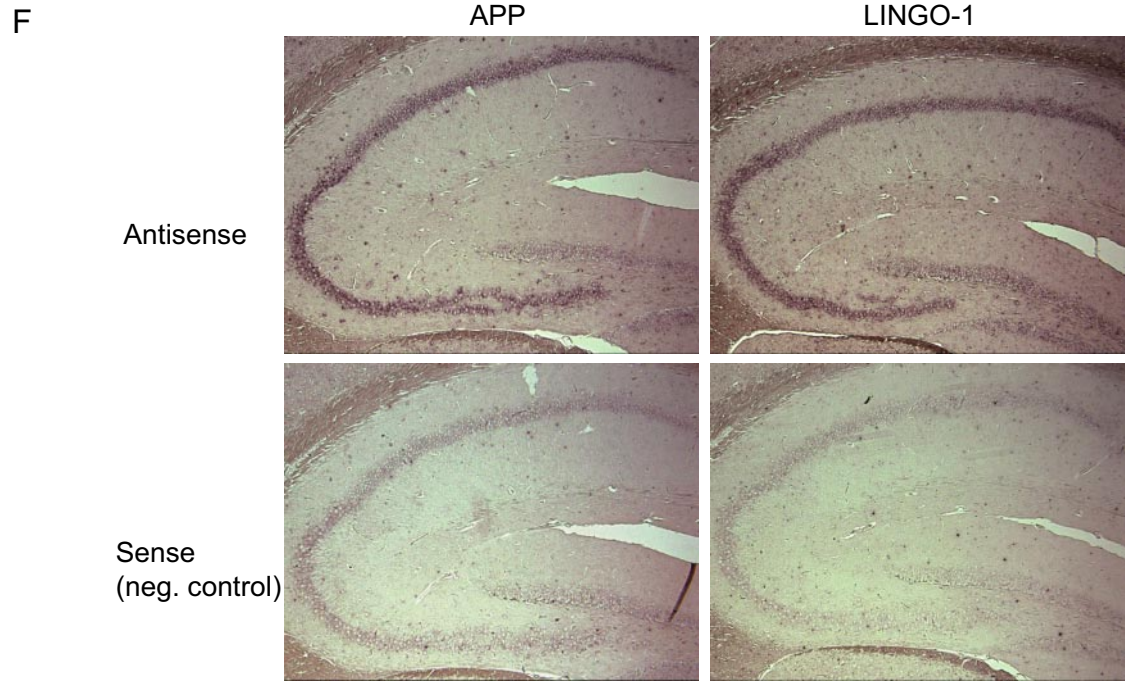
F
APP
LINGO-1
Antisense
Sense
(neg. control)

antibodies directed against APP or LINGO-1. As expected, formaldehyde cross-linking caused an overall loss of total protein (about 50%) that precipitates during ultracentrifugation as insoluble material (Fig. 5*A*). The SDS-PAGE analysis of the soluble ultracentrifugation supernatant derived from tcTPC-treated brains led to the detection of poorly resolved bands in the high molecular weight region of the gel (Fig. 5*B*) that included APP-containing cross-linked products (Fig. 5*C*). Solubilizing detergents seemed to disrupt the interaction between APP and LINGO-1 because LINGO-1 was only detectable in co-IPs derived from cross-linked brain extracts (Fig. 5*D*). Reciprocal co-IPs further supported the conclusion that LINGO-1 is associated with APP in the brain. Taken together, the above experiments confirmed binding of endogenous LINGO-1 to APP in the brain and corroborated our conceptual choice to incorporate a cross-linking step in the experimental procedure (Fig. 5*E*). LINGO-1 belongs to a subfamily of single span transmembrane proteins harboring leucine-rich repeats that also includes LINGO-2, LINGO-3, and LINGO-4. Members of this family share more than 30% sequence identity (>80% sequence homology) and have been reported to exhibit distinct expression patterns with LINGO-1 expression being largely restricted to the brain. We decided to use *in situ* hybridization (ISH) of brain sections to investigate whether there is a correlation in the expression pattern of LINGO-1 and APP in the mouse brain. Antisense ISH probes specific for both proteins showed remarkable consistency in both the distribution and relative intensity with which individual subregions in the brain were stained. No staining above background levels was observed in negative control ISH experiments in which sense strand riboprobes were used. Consistent with previous reports both LINGO-1 and APP messenger RNAs gave rise to pronounced staining of CA1 to CA3 neurons and less staining in neurons within the dentate gyrus of the hippocampus formation (Fig. 5*F*).

A subset of the physiological interactions in which APP engages have been shown to influence the relative abundances of its proteolytic cleavage products. We therefore wondered whether siRNA-mediated knockdown of LINGO-1 in a human cell line might reveal an alteration of APP proteolytic cleavages. These experiments were based on the well established HEK293 cell line that stably overexpresses APP harboring the Swedish double mutation (HEK293 APPsw) as these cells are the best suited to investigate proteolytic cleavage products of APP (34). We decided to use LINGO-1-specific quantitative RT-PCR to establish endogenous expression of LINGO-1 in HEK293 APPsw cells and identify a pool of siRNAs that mediated efficient knockdown of endogenous LINGO-1 in these cells (Fig. 6*A*). A Western blotting experiment further confirmed selective knockdown of LINGO-1 at the protein level following transient co-transfection of HEK293 APPsw cells with a full-length LINGO-1-FLAG expression construct and LINGO-1-specific siRNAs (Fig. 6*B*). Interestingly the knockdown of endogenous LINGO-1 was paralleled by a very reproducible reduction in A$\beta$ levels following harvest from the cell culture medium and analysis by a specific sandwich ELISA, *i.e.* A$\beta$ levels were reduced to 71 $\pm$ 3% (mean $\pm$ S.E.) of control levels ($n = 12$, $p < 0.001$) (Fig. 6*C*). We next wondered whether this decrease in A$\beta$ was caused by an increase in A$\beta$ clearance or a decrease in the $\beta$-cleavage C-terminal fragment of APP ($\beta$CTF; also known as C99), the proteolytic precursor of A$\beta$ (Fig. 2). Western blotting analyses of cellular extracts with antibodies directed against the C terminus of APP confirmed the latter scenario (C99 was 63 $\pm$ 3% (mean $\pm$ S.E.) of control, $n = 15$, $p < 0.001$) (Fig. 6*E*) and further established that the decrease in $\beta$CTF is paralleled by a statistically significant increase in the $\alpha$-cleavage C-terminal fragment of APP ($\alpha$CTF; also known as C83) (C83 was 170 $\pm$ 4% (mean $\pm$ S.E.) of control, $n = 6$, $p < 0.001$) (Fig. 6*D*), thereby restoring the anticipated overall balance of APP-derived fragments. To further rule out that these observations represented off-target effects of the cellular siRNA knockdown machinery, we next monitored levels of $\beta$CTF following transient overexpression of LINGO-1-FLAG in

FIG. 5. **Biochemical analyses validate benefit of cross-linking step and corroborate interaction of APP and LINGO-1.** *A*, CD-1 mice were subjected to transcardiac perfusion with PBS (*Lane 1*) or formaldehyde in PBS (*Lane 2*). Brains were rapidly dissected and homogenized in extraction buffer, and the yield of soluble protein was determined by bicinchoninic acid assay following ultracentrifugation (100,000 $\times$ *g* for 1 h at 4 °C). *B*, formaldehyde cross-linking by tcTPC causes changes in the molecular weight distribution of proteins that can be visualized by standard SDS-PAGE and Coomassie staining. Please note the increased smearing of protein bands in the *top half* of the gel commonly observed in cross-linked samples (*Lane 2*). *C*, successful formaldehyde cross-linking of APP by the tcTPC method monitored by Western blotting (*WB*) with APP-directed antibody. As expected, formaldehyde cross-linking caused a reduction in full-length uncross-linked APP protein that can be recovered in soluble form. Cross-linked products containing APP give rise to a continuous and poorly resolved smear in the high molecular mass region (>100 kDa) of the Western blot. *D*, cross-linking is essential for the detection of the interaction between APP and LINGO-1 by co-IP. Extracts generated for *A* were subjected to co-IP with mouse monoclonal APP-directed antibody (M3.2). Despite successful IP of APP in both uncross-linked (*Lane 2*) and cross-linked samples (*Lane 3*), LINGO-1 is only detectable in IP eluates derived from cross-linked brain extracts (*Lane 3*). *E*, reciprocal co-IP further corroborated interaction of APP and LINGO-1. Following transcardiac perfusion of CD-1 mice a polyclonal LINGO-1 antibody was used to co-IP LINGO-1 and interacting proteins. Western blotting analysis led to robust detection of endogenous LINGO-1 and APP in IP eluate fraction (*Lane 5*). In contrast, a control IP carried out alongside with unspecific rabbit IgG did not immunoprecipitate LINGO-1 and gave rise to only a weak signal when probed with the APP-specific antibody (*Lane 4*). *F*, *in situ* hybridization reveals strong regional correlation of APP and LINGO-1 mRNA transcription in mouse brain. Antisense and sense cRNA probes specific for APP and LINGO-1 were hybridized to hippocampus formation of wild-type C57/B6 mice. Sections were not counterstained, and *blue staining* from nitro blue tetrazolium/5-bromo-4-chloro-3-indolyl phosphate substrate represents hybridization to mRNA. *neg.*, negative.

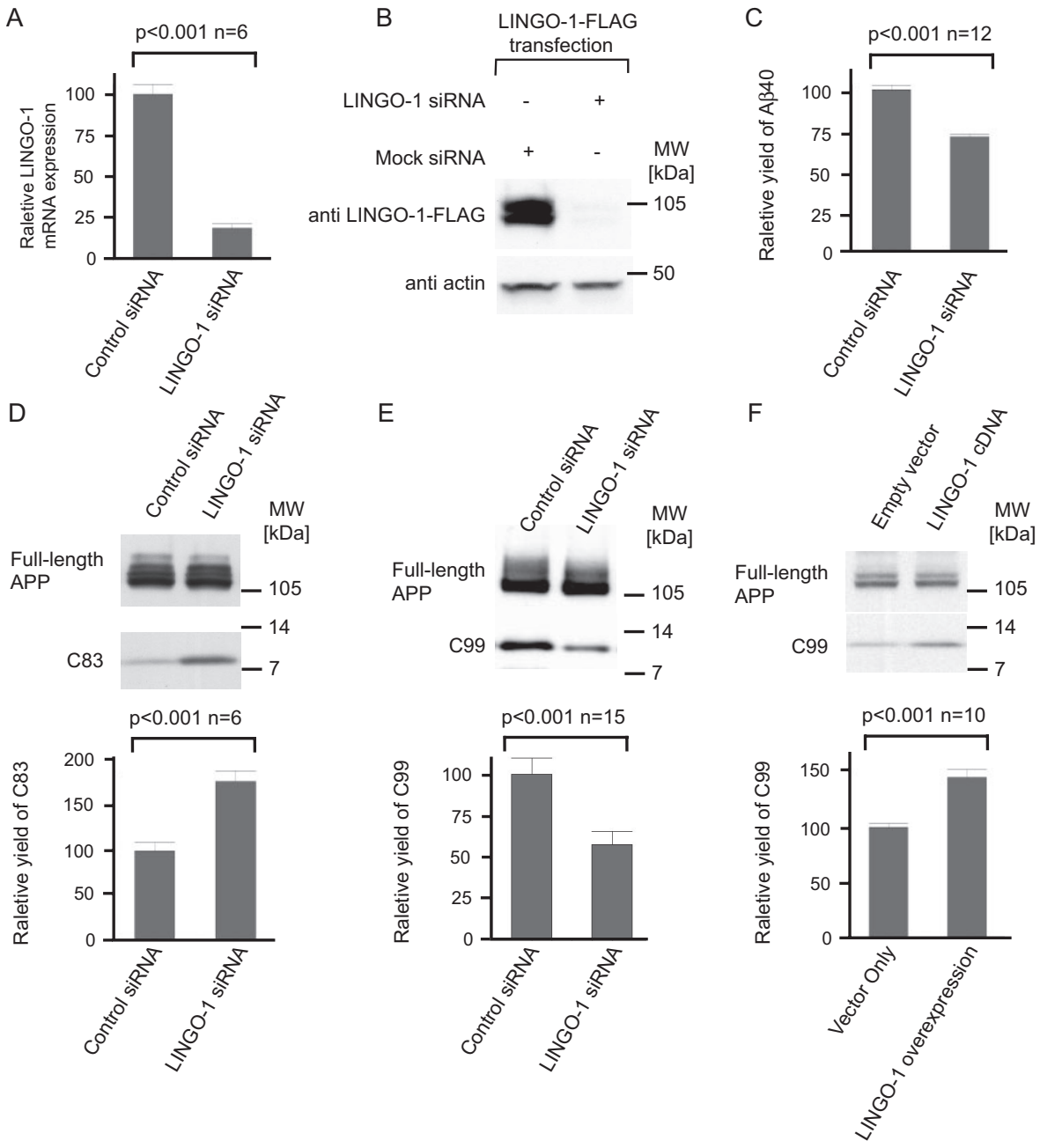


FIG. 6. **LINGO-1 affects A$\beta$ levels by influencing competing APP cleavage reactions mediated by $\alpha$- and $\beta$-secretases.** *A*, quantitative RT-PCR confirmed knockdown of endogenous LINGO-1 at the mRNA level. The *bar diagram*, which summarizes data from three independent biological repetitions and two non-overlapping LRRN6a-specific primer pairs (Lingo-1-A and Lingo-1-B), confirmed knockdown of endogenous LRRN6a to about 0.15 of the levels observed following transfection with unspecific mock siRNA. *B*, Western blotting establishes efficient knockdown of LINGO-1 protein in HEK293 APPsw cells. To verify knockdown of LINGO-1 at the protein level HEK293 APPsw cells were transiently co-transfected with an expression vector encoding for LINGO-1-FLAG and either a pool of LINGO-1-specific knockdown siRNAs or a pool of unspecific siRNAs. *C*, siRNA knockdown of endogenous LINGO-1 is paralleled by reduction in A$\beta$ secreted from HEK293 APPsw cells. HEK293 APPsw cells were transiently transfected with a pool of LINGO-1-specific siRNAs. A$\beta$ levels determined by a highly sensitive sandwich ELISA revealed statistically significant ($p < 0.001$) reduction of A$\beta$ levels of more than 25% (71 $\pm$ 3% (mean $\pm$ S.E.)). *D*, reduction of endogenous LINGO-1 levels by siRNA is paralleled by a selective increase in the levels of the $\alpha$-secretase cleavage product C83 (170 $\pm$ 4% (mean $\pm$ S.E.)). Yet the increase in C83 levels is not paralleled by changes in the expression level of full-length APP. *E*, reduction of LINGO-1 levels by treatment of HEK293 APPsw cells with a pool of LINGO-1-specific siRNAs is paralleled by a reduction (63 $\pm$ 3% (mean S.E.)) in levels of the $\beta$-secretase cleavage product C99. Again no change is observed in levels of full-length APP. *F*, overexpression of LINGO-1-FLAG in HEK293 APPsw cells is paralleled by an increase in C99 levels (131 $\pm$ 3.4% (mean $\pm$ S.E.)). Please note that all observations were statistically significant with a $p$ value $<0.001$. The recognition of C83 and C99 fragments was based on their distinct molecular weight and Western blotting with 6E10, an antibody that recognizes the C99 proteolytic APP fragment but not C83 (not shown).

HEK293 cells. Further substantiating the notion of a direct correlation of βCTF and LINGO-1, this experimental setup achieved the anticipated opposite effect on βCTF, *i.e.* overexpression of LINGO-1 in these cells was paralleled by a robust 30% increase in βCTF (C99 was 131 ± 3.4% (mean ± S.E.) of control, $n = 10$, $p < 0.001$) (Fig. 6*F*).

## DISCUSSION

A critical requirement for meaningful downstream validation studies of any interactome dataset is that the bait protein is not only represented but gives rise to the strongest protein identification in terms of both signal intensities of parent ions and percent protein coverage. It further is helpful to sort proteins according to sequence coverage obtained as this parameter often is a good correlate for the abundance and relative stability of a protein interaction. With regard to the predicted nature and size of datasets it is reasonable to assume that any target protein may engage in interactions with proteins that facilitate its formation, transport, post-translational modification, cellular function, and degradation. Finally with a well studied protein such as APP a meaningful interactome dataset would be expected to contain at least a subset of proteins for which interactions with the bait protein had previously been established by alternative means. We were encouraged to find that the interactome data presented here not only fulfilled all the above criteria but were also essentially devoid of proteins to which the bait proteins studied here should not normally have access to in a compartmentalized cell. We largely attribute the relative "cleanliness" of the APP interactome presented here, which strongly contrasts some much larger interactome datasets published in recent literature, to the stringent washing conditions that could be used following the cross-linking step.

We nevertheless expect that only a subset of proteins on the list of potential APP binding partners are *bona fide* interactors that are important for the biology of APP. Others might reside in spatial proximity to APP *in vivo* without affecting its biology. Furthermore it is conceivable that not all proteins on this list were directly cross-linked to APP. The degree of cross-linking conferred by tcTPC clearly was limited as it did not interfere with (i) independent immunoprecipitation of APP from cross-linked complexes with two different antibodies, (ii) efficient tryptic digestion of cross-linked complexes, or (iii) tandem mass spectrometry-based identifications of complex components that generally were derived from CID spectra showing extensive stretches of unmodified amino acids. To our knowledge, there is no technical element in this procedure that would favor a certain class of target proteins; therefore, we suggest that the absence of known APP interactors, such as the proteolytically active secretases and FE65, in our dataset might be due to the short lived nature of their interactions, a lack of exposed side chains that could be cross-linked by formaldehyde, or competition of interactor and APP-specific antibody for the same binding site within APP. Whether such interactions would be captured by tcTPC if larger quantities of brain tissue or longer reaction times were used remains to be determined.

*APP and ER-resident Chaperones*—As maturation of APP occurs during its passage through the secretory pathway, we expected to find various ER- and Golgi-resident proteins in our APP-specific dataset. Indeed binding of APP to various members of ER-resident chaperones had been reported previously in various contexts (35–39). Intriguingly our APP dataset not only contained a few ER chaperones but was populated by an astonishing number of proteins known to participate in various aspects of ER-based folding and the unfolded protein response. It is tempting to attribute this observation to the notorious tendency of chaperones to show up in various affinity purification eluates as a result of unspecific binding. However, to our surprise, we did not see a similar representation of chaperones in the side-by-side collected APLP1- and APLP2-specific datasets (Tables II and III) despite the high degree of homology between these proteins, and the quantitative iTRAQ comparison of IP datasets (Table IV) argues against sampling bias as the underlying cause for this observation. Further investigations are needed to reveal whether interactions of APP with ER chaperones merely provide better substrates for cross-link reactions or whether the cell dispatches an extensive armor of chaperones to APP to avoid detrimental effects that may ensue if APP maturation goes wrong.

*In Vivo Interactions of APP, APLP1, and APLP2*—Extensive studies in various knock-out models strongly argued for genetic interactions among mammalian APP family proteins. Genetic studies further suggested at least some distinct physiological roles for APLP2 and APP and established that APLP2 gene ablation contributes most strongly to double knock-out phenotypes (19, 20, 22). A direct biochemical interaction, however, had not been reported until recently when it was shown that APP can engage in homo- and heterodimerization with its mammalian homologs (17). The independent presence of APLP1 and APLP2 in both APP-directed co-immunoprecipitation datasets presented here corroborates these observations and establishes biochemical interaction of these proteins also in the living brain. Please note that this conclusion could not be firmly drawn if we had based our interactome analysis solely on the APP C terminus-directed antibody as this antibody was raised against a C-terminal fragment of APP that over its length shows weak similarity to homologous regions within APLP1 and APLP2. The extracellular domain-specific APP antibody, however, was raised against a short internal APP sequence for which no equivalent can be found in APLP1 and APLP2, thereby strongly arguing against antibody cross-reactivity as the explanation for this observation. Assuming the interaction of APP and APLP2 is functionally relevant, insights into the biology of APP may be derived from studying the interactome of APLP1 and -2. For example our observation that APP did not cross-link to kinesin-1 but may

have access to a similar motor protein of the kinesin family, Kif-1A, through its interaction with APLP2 might be of interest for investigations surrounding this controversial issue (13, 14).

*Other Previously Reported Interactions*—Our data also corroborate previous reports on interactions of APP with other proteins. In a previous tcTPC interactome dataset of the PrP we reported the presence of APP in the vicinity of PrP and NCAM (23). During the preparation of this manuscript, an involvement of PrP in the regulation of $\beta$-secretase-mediated APP cleavage was reported (40). Genetic and biochemical evidence has linked fasciclin II and the insect APP ortholog APP-like (APPL) to a common regulatory pathway involved in synapse formation (41). NCAM1 and the grasshopper protein fasciclin II share 28% amino acid identity over the entire extracellular domain suggesting that insect fasciclin II and vertebrate NCAMs probably evolved from a common ancestral molecule. The here reported binding of NCAM1 to APP may thus represent a meaningful cellular event conserved throughout evolution. We also found strong CIDs for calsyntenins, also known as alcadeins, a novel family of proteins known to associate with APP in the brain by forming a tripartite complex with X11L (42, 43). Finally our dataset contains cystatin C, an extracellular protease inhibitor reported previously to co-deposit with A$\beta$ in brain arteriolar walls (44) and AD amyloid plaques (45). Co-deposition of cystatin C with A$\beta$ was also observed in hereditary cerebral hemorrhage with amyloidosis-Dutch type, a cerebrovascular amyloidosis caused by a rare mutation within APP (46, 47), and in transgenic mice overexpressing the Swedish APP double mutation (48). Cystatin C has also been implicated in APP biology by independent studies that suggested genetic association between polymorphisms in the coding region of the cystatin C gene and late onset AD (49–52).

One previous attempt to map APP interactors by combining large scale co-immunoprecipitations with two-dimensional gel separation of candidate interactors and downstream protein identification by mass spectrometry has been reported (53). The authors separated IP eluates on a two-dimensional gel followed by in-gel trypsinization of candidate bands and reported the identification of 21 proteins that co-immunoprecipitated with APP-directed antibodies. Although the significance of candidate interactors remains unclear it is of concern that half of the reported proteins in that study were found in our unspecific mock pulldown dataset (for example tubulin, Munc18, actin, 14-3-3, myelin basic protein, and glial fibrillary acidic protein), and the most strongly represented protein was not APP but tubulin.

*Similarities in the Biology of APP and p75*—Following the logic of "guilt by association," the cellular function of a protein can frequently be inferred from its next neighbor relationship with other proteins of known function (54). When viewed from this angle our data support the notion that APP protein family members may play a role in neuritogenesis (LINGO-1, mental disorder-associated GTPase activating protein (MEGAP), reticulon, and neurofascin), cell adhesion (Thy-1, NCAM1, and contactin), and synapse formation (GABA-B1a and NCAM1; see below).

Also our data consolidated intriguing parallels in the biology of APP and p75. Like APP, p75 has been shown recently to represent an $\alpha$- and $\gamma$-secretase substrate (54–57). APP as well as p75 has also been repeatedly proposed to localize to rafts, specialized membrane regions enriched in GPI-anchored proteins, cholesterol, and sphingolipids (58). The presence of four well known GPI-anchored molecules, contactin, Thy-1, PrP, and NCAM1-GPI, in the APP interactome presented here is in agreement with this notion. Both APP and p75 appear to be directed by Vps10p domain-containing retromer proteins into recycling pathways (15, 16, 59). Although p75 serves as a receptor for nerve growth factor, the equivalent extracellular ligand for APP remains unclear. Our data, however, further corroborate the previously reported interaction of F-spondin as a physiological extracellular ligand for APP (3) and suggest that APP may indirectly have access to VGF8a through its interaction with APLP1. Our data also establish LINGO-1, alias LRRN6a, as an APP-interacting protein. To our knowledge, the only other proteins known to interact with LINGO-1 are Taj/Troy and, again, p75 (60). Apparently to promote axonal branching and regeneration, p75 engages in heterotrimeric interactions with LINGO-1 and the GPI-anchored Nogo receptor (61). It has been shown previously that ligands of this receptor complex, reticulons 1–4, influence the level of BACE1-mediated A$\beta$ generation (62). It has further been shown that both p75 itself and the Nogo receptor, another protein harboring leucine-rich-repeat domains, affect APP processing (63–65). However, whereas there is an inverse relationship between Nogo receptor and secreted A$\beta$ levels, LINGO-1 appears to promote A$\beta$ secretion. Finally the heterotrimeric complex containing p75 mediates its biological effects through activation of the small GTPase rho (66). Our APP interactome map also includes a strong hit for srGAP3, alias MEGAP, a rho-activating protein, and suggests that APP may have indirect access to rho through its interaction with APLP2 (Table III). Interestingly both srGAP3, short for slit-robo GTPase-activating protein 3, and LINGO-1 have been implicated in slit-robo-like signaling in the brain. In fact, LINGO-1 was originally discovered in a sequence database search for human slit orthologs selectively expressed in brain (61). Please note that LINGO-1 and srGAP3 were identified in this work in independent IPs with APP-specific antibodies directed against extracellular and intercellular domains, respectively.

*LINGO-1 and LRRTM3*—During the preparation of this manuscript a study was published that reported on the identification of a novel APP interactor, LRRTM3, identified based on a genomic *in vitro* siRNA screen for genes that regulate APP processing in HEK293T cells (67). Interestingly LRRTM3 belongs to the same protein superfamily of leucine-rich repeat (LRR) domain-harboring proteins as LINGO-1, and as such

the two proteins display considerable sequence similarity (27.1% sequence similarity and 17.7% sequence identity). Clearly the relative contribution of LRRTM3 and LINGO-1 to the biology of APP will have to be addressed in a separate study. It is noteworthy, however, that LINGO-1 and LRRTM3 appear to demonstrate an inverse expression pattern within neuronal formations of the hippocampus, *i.e.* whereas APP and LINGO-1 expression levels are high in the CA1 to CA3 region and low in the dentate gyrus, LRRTM3 expression levels are reported to be particularly high in neurons of the dentate gyrus, and only modest expression of LRRTM3 was documented in CA1 to CA3 neurons (67). Despite this disparity in expression levels, the presence of LINGO-1 or LRRTM3 appears to exert a strikingly similar effect on the processing of APP fragments in cell culture assays. It remains to be seen whether promiscuous binding of APP to a subset of LRR domain-harboring proteins in cell culture paradigms and competition of LRR-harboring proteins (Nogo receptor, LINGO-1, and LRRTM3) for binding to APP underlie some of these observations. Our data suggest a model in which LINGO-1 may facilitate access of BACE1 to APP and thereby promote cleavage at the $\beta$-cleavage site. Consistent with this hypothesis, the experimental reduction of LINGO-1 causes a reduction of both C99 and A$\beta$ fragments as well as an increase in the secretion of the $\alpha$-secretase cleavage product C83. Although our data indicate that LINGO-1 may exert this effect on APP cleavage through direct interaction, more work will be needed to gain mechanistic insights. Plausible modes of action include, but are not limited to, recruitment of APP to sites of $\beta$-secretase activity, stabilization of the enzyme-substrate complex, or inhibition of alternative cleavage by $\alpha$-secretase.

*Concluding Remarks*—In summary, this work represents the most comprehensive analysis of the APP interactome to date. It sheds light on a molecular framework of APP interactions that may underlie proposed functional roles of APP in neuritogenesis/axonal regeneration, cell adhesion, and synaptogenesis. Intensive validation work will be required to more fully appreciate the role of individual proteins in the APP network presented here. It is hoped that further investigations of this network will reveal an "Achilles' heel" in the molecular biology of APP that can be exploited for diagnostic or therapeutic purposes.

* This work was supported by Canadian Institutes for Health Research (CIHR) Grant MOP-74734, the Canadian Foundation for Innovation (CIHR Grant 10087), and National Institutes of Health Grant GM61898. The costs of publication of this article were defrayed in part by the payment of page charges. This article must therefore be hereby marked "*advertisement*" in accordance with 18 U.S.C. Section 1734 solely to indicate this fact.

[S] The on-line version of this article (available at http://www.mcponline.org) contains supplemental material.

[b] Both authors contributed equally to this work.

[c] Funded through the CIHR Strategic Program in Protein Folding.

[e] Received fellowship support (Grant 20059) from the University of Toronto.

[f] Present address: Samuel Lunenfeld Research Inst., Toronto, Ontario M5G 1X5, Canada.

[i] Supported by the Alzheimer Society of Ontario and Ontario Mental Health Foundation.

[m] Received generous support from the W. Garfield Weston Foundation. To whom correspondence should be addressed. E-mail: g.schmittulms@utoronto.ca.

REFERENCES

1. Haass, C. (2004) Take five—BACE and the $\gamma$-secretase quartet conduct Alzheimer's amyloid $\beta$ peptide generation. *EMBO J.* **23,** 483–488
2. Selkoe, D. J. (2001) Alzheimer's disease: genes, proteins, and therapy. *Physiol. Rev.* **81,** 741–766
3. Ho, A., and Sudhof, T. C. (2004) Binding of F-spondin to amyloid-$\beta$ precursor protein: a candidate amyloid-$\beta$ precursor protein ligand that modulates amyloid-$\beta$ precursor protein cleavage. *Proc. Natl. Acad. Sci. U. S. A.* **101,** 2548–2553
4. Nishimoto, I., Okamoto, T., Matsuura, Y., Takahashi, S., Murayama, Y., and Ogata, E. (1993) Alzheimer amyloid protein precursor complexes with brain GTP-binding protein $G_o$. *Nature* **362,** 75–79
5. Borg, J. P., Ooi, J., Levy, E., and Margolis, B. (1996) The phosphotyrosine interaction domains of X11 and FE65 bind to distinct sites on the YENPTY motif of amyloid precursor protein. *Mol. Cell. Biol.* **16,** 6229–6241
6. Fiore, F., Zambrano, N., Minopoli, N., Donini, G., Duilio, A., and Russo, T. (1995) The regions of the Fe65 protein homologous to the phosphotyrosine interaction/phosphotyrosine binding domain of SHc bind the intracellular domain of the Alzheimer's amyloid precursor protein. *J. Biol. Chem.* **270,** 30853–30856
7. Trommsdorff, M., Borg, J. P., Margolis, B., and Herz, J. (1998) Interaction of cytosolic adaptor proteins with neuronal apolipoprotein E receptors and the amyloid precursor protein. *J. Biol. Chem.* **273,** 33556–33560
8. Van Gassen, G., Annaert, W., and Van Broeckhoven, C. (2000) Binding partners of Alzheimer's disease proteins: are they physiologically relevant? *Neurobiol. Dis.* **7,** 135–151
9. Kimberly, W. T., Zheng, J. B., Guenette, S. Y., and Selkoe, D. J. (2001) The intracellular domain of the $\beta$-amyloid precursor protein is stabilized by Fe65 and translocates to the nucleus in a notch-like manner. *J. Biol. Chem.* **276,** 40288–40292
10. Zheng, P., Eastman, J., Pol, S. V., and Pimplikar, S. W. (1998) PAT1, a microtubule-interacting protein, recognizes the basolateral sorting signal of amyloid precursor protein. *Proc. Natl. Acad. Sci. U. S. A.* **95,** 14745–14750
11. Kamal, A., Almenar-Queralt, A., LeBlanc, J. F., Roberts, E. A., and Goldstein, L. S. (2001) Kinesin-mediated axonal transport of a membrane compartment containing $\beta$-secretase and presenilin-1 requires APP. *Nature* **414,** 643–648
12. Kamal, A., Stokin, G. B., Yang, Z., Xia, C. H., and Goldstein, L. S. (2000) Axonal transport of amyloid precursor protein is mediated by direct binding to the kinesin light chain subunit of kinesin-1. *Neuron* **28,** 449–459
13. Stokin, G. B., Lillo, C., Falzone, T. L., Brusch, R. G., Rockenstein, E., Mount, S. L., Raman, R., Davies, P., Masliah, E., Williams, D. S., and Goldstein, L. S. (2005) Axonopathy and transport deficits early in the pathogenesis of Alzheimer's disease. *Science* **307,** 1282–1288
14. Lazarov, O., Morfini, G. A., Lee, E. B., Farah, M. H., Szodorai, A., DeBoer, S. R., Koliatsos, V. E., Kins, S., Lee, V. M., Wong, P. C., Price, D. L., Brady, S. T., and Sisodia, S. S. (2005) Axonal transport, amyloid precursor protein, kineasin-1 and the processing apparatus: revisited. *J. Neurosci.* **25,** 2386–2395
15. Andersen, O. M., Reiche, J., Schmidt, V., Gotthardt, M., Spoelgen, R., Behlke, J., Von Arnim, C. A., Breiderhoff, T., Jansen, P., Wu, X., Bales, K. R., Cappai, R., Masters, C. L., Gliemann, J., Mufson, E. J., Hyman, B. T., Paul, S. M., Nykjaer, A., and Willnow, T. E. (2005) Neuronal sorting protein-related receptor sorLA/LR11 regulates processing of the amyloid precursor protein. *Proc. Natl. Acad. Sci. U. S. A.* **102,** 13461–13466
16. Rogaeva, E., Meng, Y., Lee, J. H., Gu, Y., Kawarai, T., Zou, F., Katayama, T., Baldwin, C. T., Cheng, R., Hasegawa, H., Chen, F., Shibata, N., Lunetta, K. L., Pardossi-Piquard, R., Boehm, C., Wakutani, Y., Cupples, A. L., Cuenco, K. T., Green, R., Pinessi, L., Rainero, I., Sorbi, S., Bruni, A.,

Duara, R., Friedland, R., Inzelberg, R., Hampe, W., Bujo, H., Song, Y.-Q., Fraser, P. E., Andersen, O., Graff-Radford, N., Petersen, R., Dickson, D., Der, S. D., Fraser, P., Schmitt-Ulms, G., Younkin, S., Mayeux, R., Farrer, L., and St. George-Hyslop, P. (2007) The neuronal sortilin-related receptor SORL1 is genetically associated with Alzheimer disease. *Nat. Genet.* **39,** 168–177

17. Soba, P., Eggert, S., Wagner, K., Zentgraf, H., Siehl, K., Kreger, S., Lower, A., Langer, A., Merdes, G., Paro, R., Masters, C. L., Muller, U., Kins, S., and Beyreuther, K. (2005) Homo- and heterodimerization of APP family members promotes intercellular adhesion. *EMBO J.* **24,** 3624–3634
18. Reinhard, C., Hebert, S. S., and De Strooper, B. (2005) The amyloid-$\beta$ precursor protein: integrating structure with biological function. *EMBO J.* **24,** 3996–4006
19. Heber, S., Herms, J., Gajic, V., Hainfellner, J., Aguzz, A., Rulicke, T., von Kretzschmar, H., von Koch, C., Sisodia, S. S., Tremml, P., Lipp, H. P., Wofer, D. P., and Muller, U. (2000) Mice with combined gene knock-outs reveal essential and partially redundant functions of amyloid precursor protein family members. *J. Neurosci.* **20,** 7951–7963
20. Herms, J., Aniker, B., Heber, S., Ring, S., Fuhrmann, M., Kretzschmar, H., Sisodia, S. S., and Muller, U. (2004) Cortical dysplasia resembling human type 2 lissencephaly in mice lacking all three APP family members. *EMBO J.* **23,** 4106–4115
21. Leyssen, M., Ayaz, D., Herbert, S. S., Reeve, S., De Strooper, B., and Hassan, B. A. (2005) Amyloid precursor protein promotes post-developmental neurite arborization in the Drosophila brain. *EMBO J.* **24,** 2944–2955
22. Zheng, H., Jiang, M., Trumbauer, M. E., Sirinathsinghji, D. J., Hopkins, R., Smith, D. W., Heavens, R. P., Dawson, G. R., Boyce, S., and Conner, M. W. (1995) $\beta$-Amyloid precursor protein-deficient mice show reactive gliosis and decreased locomotor activity. *Cell* **81,** 525–531
23. Schmitt-Ulms, G., Hansen, K., Liu, J., Cowdrey, C., Yang, J., DeArmond, S., Cohen, F. E., Prusiner, S. B., and Baldwin, M. A. (2004) Time-controlled transcardiac perfusion crosslinking for the study of protein interactions in complex tissues. *Nat. Biotechnol.* **22,** 724–731
24. Thinakaran, G., Kitt, C. A., Roskams, A. J., Slunt, H. H., Masliah, E., von Koch, C., Ginsberg, S. D., Ronnett, G. V., Reed, R. R., and Price, D. L. (1995) Distribution of an APP homolog, APLP2, in the mouse olfactory system: a potential role for APLP2 in axogenesis. *J. Neurosci.* **15,** 6314–6326
25. Rappsilber, J., Ishihama, Y., and Mann, M. (2003) Stop and go extraction tips for matrix-assisted laser desorption/ionization, nanoelectrospray, and LC/MS sample pretreatment in proteomics. *Anal. Chem.* **75,** 663–670
26. Chalkley, R. J., Baker, P. R., Huang, L., Hansen, K. C., Allen, N. P., Rexach, M., and Burlingame, A. L. (2005) Comprehensive analysis of a multidimensional liquid chromatography mass spectrometry dataset acquired on a quadrupole selecting quadrupole collision cell, time-of-flight mass spectrometer. II. New developments in Protein Prospector allow for reliable and comprehensive automatic analysis of large datasets. *Mol. Cell. Proteomics* **4,** 1194–1204
27. Perkins, D. N., Pappin, D. J., Creasy, D. M., and Cottrell, J. S. (1999) Probability-based protein identification by searching sequence databases using mass spectrometry data. *Electrophoresis* **20,** 3551–3567
28. Mann, M., and Wilm, M. (1994) Error-tolerant identification of peptides in sequence databases by peptides sequence tags. *Anal. Chem.* **66,** 4390–4399
29. Yu, G. (2000) A novel protein (nicastrin) modulates presenilin-mediated Notch/Glp1 and $\beta$APP processing. *Nature* **407,** 48–54
30. Chen, F. (2002) Presenilin 1 mutations activate $\gamma$42-secretase but reciprocally inhibit $\varepsilon$-secretase cleavage of amyloid precursor protein (APP) and S3-cleavage of notch. *J. Biol. Chem.* **277,** 36521–36526
31. Liu, H., Sadygov, R. G., and Yates, J. R. (2004) A model for random sampling and estimation of relative protein abundance in shotgun proteomics. *Anal. Chem.* **76,** 4193–4201
32. Steen, H., and Mann, M. (2004) The ABC's (and XYZ's) of peptide sequencing. *Nat. Rev. Mol. Cell Biol.* **5,** 699–711
33. Tabb, D. L., MacCross, M. J., Wu, C. C., Anderson, S. D., and Yates, J. R. (2003) Similarity among tandem mass spectra from proteomics experiments: detection, significance, and utility. *Anal. Chem.* **75,** 2470–2477
34. Chen, F., Hasegawa, H., Schmitt-Ulms, G., Kawarai, T., Bohm, C., Katayama, T., Gu, Y., Sanjo, N., Glista, M., Rogaeva, E., Wakutani, Y., Pardossi-Piquard, R., Ruan, X., Tandon, A., Checler, F., Marambaud, P., Hansen, K., Westaway, D., St. George-Hyslop, P. H., and Fraser, P. (2006) TMP21 is a presenilin complex component that modulates $\gamma$-secretase but not $\varepsilon$-secretase activity. *Nature* **440,** 1208–1212
35. Erickson, R. R., Dunning, L. M., Olson, D. A., Cohen, S. J., Davis, A. T., Wood, W. G., Kratzke, R. A., and Holtzman, J. L. (2005) In cerebrospinal fluid ER chaperones ERp57 and calreticulin bind $\beta$-amyloid. *Biochem. Biophys. Res. Commun.* **332,** 50–57
36. Johnson, R. J., Xiao, G., Shanmugaratnam, J., and Fine, R. E. (2001) Calreticulin functions as a molecular chaperone for the $\beta$-amyloid precursor protein. *Neurobiol. Aging* **22,** 387–395
37. Kogel, D., Schomburg, R., Schurmann, T., Reimertz, C., Konig, H. G., Poppe, M., Eckert, A., Muller, W. E., and Prehn, J. H. (2003) The amyloid precursor protein protects PC12 cells against endoplasmic reticulum stress-induced apoptosis. *J. Neurochem.* **87,** 248–256
38. Vattemi, G., Engel, K., McFerrin, J., and Askanas, V. (2004) Endoplasmic reticulum stress and unfolded protein response in inclusion body myositis muscle. *Am. J. Pathol.* **164,** 1–7
39. Yang, Y., Turner, R. S., and Gaut, J. R. (1998) The chaperone BiP/GRP78 binds to amyloid precursor protein and decreases A$\beta$40 and A$\beta$42 secretion. *J. Biol. Chem.* **273,** 25552–25555
40. Parkin, E. T., Watt, N. T., Hussain, I., Eckman, E. A., Eckman, C. B., Manson, J. C., Baybutt, H. N., Turner, A. J., and Hooper, N. M. (2007) Cellular prion protein regulates $\beta$-secretase cleavage of the Alzheimer's amyloid precursor protein. *Proc. Natl. Acad. Sci. U. S. A.* **104,** 11062–11067
41. Ashley, J., Packard, M., Ataman, B., and Budnik, V. (2005) Fasciclin II signals new synapse formation through amyloid precursor protein and the scaffolding protein dX11/Mint. *J. Neurosci.* **25,** 5943–5955
42. Araki, Y., Miyagi, N., Kato, N., Yoshida, T., Wada, S., Nishimura, M., Komano, H., Yamamoto, T., De Strooper, B., Yamamoto, K., and Suzuki, T. (2004) Coordinated metabolism of alcadein and amyloid $\beta$-protein precursor regulates FE65-dependent gene transactivation. *J. Biol. Chem.* **279,** 24343–24354
43. Araki, Y., Tomita, S., Yamaguchi, H., Miyagi, N., Sumioka, A., Kirino, Y., and Suzuki, T. (2003) Novel cadherin-related membrane proteins, alcadeins, enhance the X11-like protein-mediated stabilization of amyloid $\beta$-protein precursor metabolism. *J. Biol. Chem.* **278,** 49448–49458
44. Vinters, H. V., Nishimura, G. S., Secor, D. L., and Pardridge, W. M. (1990) Immunoreactive A4 and gamma-trace peptide colocalization in amyloidotic arteriolar lesions in brains of patients with Alzheimer's disease. *Am. J. Pathol.* **137,** 233–240
45. Sastre, M., Calero, M., Pawlik, M., Mathews, P. M., Kumar, A., Danilov, V., Schmidt, S. D., Nixon, R. A., Frangione, B., and Levy, E. (2004) Binding of cystatin C to Alzheimer's amyloid $\beta$ inhibits in vitro amyloid formation. *Neurobiol. Aging* **25,** 1033–1043
46. Bornebroek, M., Haan, J., Maat-Schieman, M. L., Van Duinen, S. G., and Roos, R. A. (1996) Hereditary cerebral hemorrhage with amyloidosis-Dutch type (HCHWA-D). I. A review of clinical, radiologic and genetic aspects. *Brain Pathol.* **6,** 111–114
47. Maat-Schieman, M. L., Van Diunen, S. G., Bornebroek, M., Haan, J., and Roos, R. A. (1996) Hereditary cerebral hemorrhage with amyloidosis-Dutch type (HCHWA-D). II. A review of histopathological aspects. *Brain Pathol.* **6,** 115–120
48. Steinhoff, T., Moritz, E., Wollmer, M. A., Mohajeri, M. H., Kins, S., and Nitsch, R. M. (2001) Increased cystatin C in astrocytes of transgenic mice expressing the K670N-M671L mutation of the amyloid precursor protein and deposition in brain amyloid plaques. *Neurobiol. Dis.* **8,** 647–654
49. Beyer, K., Lao, J. L., Gomez, M., Riutort, N., Latorre, P., Mate, J. L., and Ariza, A. (2001) Alzheimer's disease and the cystatin C gene polymorphism: an association study. *Neurosci. Lett.* **315,** 17–20
50. Crawford, F. C., Freeman, M. J., Schinka, J. A., Abdullah, L. I., Gold, M., Hartman, R., Krivian, K., Morris, M. D., Richards, D., Duara, R., Anand, R., and Mullan, M. J. (2000) A polymorphism in the cystatin C gene is a novel risk factor for late-onset Alzheimer's disease. *Neurology* **55,** 763–768
51. Finckh, U., Von der Kammer, H., Velden, J., Michel, T., Andresen, B., Deng, A., and Zhang, J. (2000) Genetic association of a cystatin C gene polymorphism with late-onset Alzheimer disease. *Arch. Neurol.* **57,** 1579–1583
52. Olson, J. M., Goddard, K. A., and Dudek, D. M. (2002) A second locus for

very-late-onset Alzheimer disease: a genome scan reveals linkage to 20p and epistasis between 20p and the amyloid precursor protein region. *Am. J. Hum. Genet.* **71,** 154–161
53. Cottrell, B., Galvan, V., Banwait, S., Gorostiza, O., Lombardo, C., Williams, T., Schilling, B., Peel, A., Gibson, B., Koo, E. H., Link, C. D., and Bredesen, D. E. (2005) A pilot proteomic study of amyloid precursor interactors in Alzheimer's disease. *Ann. Neurol.* **58,** 277–289
54. Vazquez, A., Flammini, A., Maritan, A., and Vespignani, A. (2003) Global protein function prediction from protein-protein interaction networks. *Nat. Biotechnol.* **21,** 697–700
55. Domeniconi, M., Zampieri, N., Spencer, T., Hilaire, M., Mellado, W., Chao, M. V., and Filbin, M. T. (2005) MAG induces regulated intramembrane proteolysis of the p75 neurotrophin receptor to inhibit neurite outgrowth. *Neuron* **46,** 839–840
56. Kanning, K. C., Hudson, M., Amieux, P. S., Wiley, J. C., Bothwell, M., and Schecterson, L. C. (2003) Proteolytic processing of the p75 neurotrophin receptor and two homologs generates C-terminal fragments with signaling capability. *J. Neurosci.* **23,** 5424–5436
57. Zampieri, N., Xu, C. F., Neubert, T. A., and Chao, M. V. (2005) Cleavage of p75 neurotrophin receptor by $\alpha$-secretase and $\gamma$-secretase requires specific receptor domains. *J. Biol. Chem.* **280,** 14563–14571
58. Yu, W., Guo, W., and Feng, L. (2004) Segregation of Nogo66 receptors into lipid rafts in rat brain and inhibition of Nogo66 signaling by cholesterol depletion. *FEBS Lett.* **57,** 87–92
59. Nykjaer, A., Lee, R., Teng, K. K., Jansen, P., Madsen, P., Nielsen, M. S., Jacobsen, C., Kliemannel, M., Schwarz, E., Willnow, T. E., Hempstead, B. L., and Petersen, C. M. (2004) Sortilin is essential for proNGF-induced neuronal cell death. *Nature* **427,** 798–799
60. Shao, Z., Browning, J. L., Lee, X., Scott, M. L., Shulga-Morskaya, S., Allaire, N., Thill, G., Levesque, M., Sah, D., McCoy, J. M., Murray, B., Jung, V., Pepinsky, R. B., and Mi, S. (2005) Taj/Troy, an orphan TNF receptor family member, binds Nogo-66 receptor 1 and regulates axonal regeneration. *Neuron* **45,** 353–359
61. Mi, S., Lee, X., Shao, Z., Thill, G., Ji, B., Relton, J., Levesque, M., Allaire, N., Perrin, S., Sands, B., Crowell, T., Cate, R. L., McCoy, J. M., and Pepinsky, R. B. (2004) LINGO-1 is a component of the Nogo-66 receptor/p75 signaling complex. *Nat. Neurosci.* **7,** 221–228
62. He, W., Lu, Y., Qahwash, I., Hu, X. Y., Chang, A., and Yan, R. (2004) Reticulon family members modulate BACE1 activity and amyloid-$\beta$ peptide generation. *Nat. Med.* **10,** 959–965
63. Park, J. H., Gimbel, D. A., GrandPre, T., Lee, J. K., Kim, J. E., Li, W., Lee, D. H., and Strittmatter, S. M. (2006) Alzheimer precursor protein interaction with the Nogo-66 receptor reduces amyloid-$\beta$ plaque deposition. *J. Neurosci.* **26,** 1386–1395
64. Park, J. H., Widi, G. A., Gimbel, D. A., Harel, N. Y., Lee, D. H., and Strittmatter, S. M. (2006) Subcutaneous Nogo receptor removes brain amyloid-$\beta$ and improves spatial memory in Alzheimer's transgenic mice. *J. Neurosci.* **26,** 13279–13286
65. Costantini, C., Weindruch, R., Della Valle, G., and Puglielli, L. (2005) A TrkA-to-p75$^{NTR}$ molecular switch activates amyloid $\beta$-peptide generation during aging. *Biochem. J.* **391,** 59–67
66. Yamashita, T., Tucker, K. L., and Barde, Y. A. (1999) Neurotrophin binding to the p75 receptor modulates rho activity and axonal outgrowth. *Neuron* **24,** 585–593
67. Majercak, J., Ray, W. J., Espeseth, A., Simon, A., Shi, X. P., Wolffe, C., Getty, K., Marine, S., Stec, E., Ferrer, M., Strulovici, B., Bartz, S., Gates, A., Xu, M., Huang, Q., Ma, L., Shughrue, P., Burchard, J., Colussi, D., Pietrak, B., Kahana, J., Beher, D., Rosahl, T., Shearman, M., Hazuda, D., Sachs, A. B., Koblan, K. S., Seabrook, G. R., and Stone, D. J. (2006) LRRTM3 promotes processing of amyloid-precursor protein by BACE1 and is a positional candidate gene for late-onset Alzheimer's disease. *Proc. Natl. Acad. Sci. U. S. A.* **103,** 17967–17972